Graduate School ETD Form 9
(Revised 01/14)

PURDUE UNIVERSITY
GRADUATE SCHOOL
Thesis/Dissertation Acceptance

This is to certify that the thesis/dissertation prepared

By Ragibul Huq

Entitled
DEVELOPMENT OF A NOVEL SENSOR FOR SOOT DEPOSITION MEASUREMENT IN A DIESEL PARTICULATE FILTER USING ELECTRICAL CAPACITANCE TOMOGRAPHY

For the degree of Master of Science in Mechanical Engineering

Is approved by the final examining committee:

Sohel Anwar

Afshin Izadian

Andres Tovar

To the best of my knowledge and as understood by the student in the *Thesis/Dissertation Agreement. Publication Delay, and Certification/Disclaimer (Graduate School Form 32)*, this thesis/dissertation adheres to the provisions of Purdue University's "Policy on Integrity in Research" and the use of copyrighted material.

Sohel Anwar

Approved by Major Professor(s): _____

_____

Approved by: Sohel Anwar 07/07/2014

Head of the Department Graduate Program Date

DEVELOPMENT OF A NOVEL SENSOR FOR SOOT DEPOSITION MEASUREMENT IN A DIESEL PARTICULATE FILTER USING ELECTRICAL CAPACITANCE TOMOGRAPHY

A Thesis

Submitted to the Faculty

of

Purdue University

by

Ragibul Huq

In Partial Fulfillment of the

Requirements for the Degree

of

Master of Science in Mechanical Engineering

August 2014

Purdue University

Indianapolis, Indiana

I would like to dedicate this work to my parents Ramjul Huq and Helena Huq. I thank all of you for your love and support.

ACKNOWLEDGEMENTS

This work was supported by the Mechanical Engineering Department of Indiana University-Purdue University Indianapolis. The author gratefully acknowledges the support of Mr. Rudy Earlson, and Mr. Joseph Huerkamp Laboratory Technician of Mechanical Engineering. The author also likes to thank Mr. Edmund Hodzen, Director Advanced Controls Systems Engineering, Cummins Inc. And the author is really grateful to his supervisor Dr. Sohel Anwar for his support throughout the years.

TABLE OF CONTENTS

Page

LIST OF TABLES

LIST OF FIGURES

Figure Page

GLOSSARY

Symbol	Quantity
α	Temperature coefficient
$\mathcal{E}$	Permittivity
$\mathcal{E}_r$	Relative permittivity
$\mathcal{E}_s$	Effective permittivity in Series Permittivity Model
$\mathcal{E}_p$	Effective permittivity in Parallel Permittivity Model
$\mathcal{E}_m$	Effective permittivity in Maxwell Garnett Permittivity Model
$\mathcal{E}_b$	Relative permittivity of a base dielectric
$\mathcal{E}_i$	Relative permittivity of the i-th sort of inclusions
$\mathcal{E}_o$	in vacuum, the value of $\mathcal{E}o = 8.854 * 10\text{-}12$ F/m
ρ_T	Resistivity at temperature T
A	Electrode surface area
C	Normalized electrode-pair capacitances
C_m	Overall capacitance in Maxwell Garnett Permittivity Model
C_p	Overall capacitance in Parallel Permittivity Model
C_s	Overall capacitance in Series Permittivity Model
d	Distance between two plates
D	Flux density

Symbol	Quantity
E	Electric field strength between the plates
f_i	Volume fraction occupied by the inclusions of the i-th sort
K	Normalized pixel permittivity's matrix
N_{ik}	Depolarization factors of the i-th sort of inclusions
Q	Charge
S	Sensitivity matrix
V	Potential difference

ABSTRACT

Huq, Ragibul. M.S.M.E., Purdue University, August 2014. Development of a Novel Sensor for Soot Deposition Measurement in a Diesel Particulate Filter Using Electrical Capacitance Tomography. Major Professor: Sohel Anwar.

This paper presents a novel approach of particulate material (soot) measurement in a Diesel particulate filter using Electrical Capacitance Tomography. Modern Diesel Engines are equipped with Diesel Particulate Filters (DPF), as well as on-board technologies to evaluate the status of DPF because complete knowledge of DPF soot loading is very critical for robust efficient operation of the engine exhaust after treatment system. Emission regulations imposed upon all internal combustion engines including Diesel engines on gaseous as well as particulates (soot) emissions by Environment Regulatory Agencies. In course of time, soot will be deposited inside the DPFs which tend to clog the filter and hence generate a back pressure in the exhaust system, negatively impacting the fuel efficiency. To remove the soot build-up, regeneration of the DPF must be done as an engine exhaust after treatment process at pre-determined time intervals. Passive regeneration use exhaust heat and catalyst to burn the deposited soot but active regeneration use external energy in such as injection of diesel into an upstream DOC to burn the soot. Since the regeneration process consume fuel, a robust and efficient operation based on accurate knowledge of the particulate matter deposit (or soot load)

becomes essential in order to keep the fuel consumption at a minimum. In this paper, we propose a sensing method for a DPF that can accurately measure in-situ soot load using Electrical Capacitance Tomography (ECT). Simulation results show that the proposed method offers an effective way to accurately estimate the soot load in DPF. The proposed method is expected to have a profound impact in improving overall PM filtering efficiency (and thereby fuel efficiency), and durability of a Diesel Particulate Filter (DPF) through appropriate closed loop regeneration operation.

1. INTRODUCTION AND LITERATURE REVIEW

1.1 Introduction

Particulate matter also known as particle pollution or soot is a complex mixture of extremely small particles and liquid droplets. Particle pollution is made up of a number of components, including acids (such as nitrates and sulfates), organic chemicals, metals, and soil or dust particles. The size of particles is directly linked to their potential for causing health problems. United States Environment Protection Agency (US EPA) is concerned about particles that are 10 micrometers in diameter or smaller because those are the particles that generally pass through the throat and nose and enter the lungs according to EPA website, and once inhaled, these particles can affect the heart and lungs and cause serious health effects [1].

The issues of global climatic changes and human health hazards caused by different types of pollutions led environment protection agencies to identify the scopes of improvement and make the regulations more rigorous. With increasingly stringent emission regulations novel diesel engines have come a long way in the area of emission control technologies in the reduction of particulate matter emissions via diesel particulate filter or DPF.

Diesel particulate filters were first used in the 1980 which remove the particulate matter/ soot from the exhaust of the Diesel engine with an efficiency level of 90-99% or

more. The most commonly used DPFs are porous ceramic wall-flow filters, as shown schematically in Figure 1.1. Refractory materials such as Silicon Carbide, Cordierite or Aluminum-Titanate are used for this purpose [2]. Silicon carbide filters dominate the market owing to the material's mechanical strength and high thermal stability [3]. Alternate channels are plugged, forcing the exhaust through the porous channel walls. The gaseous exhaust passes through the porous walls, but Particulate Matter (PM) is trapped in the filter.

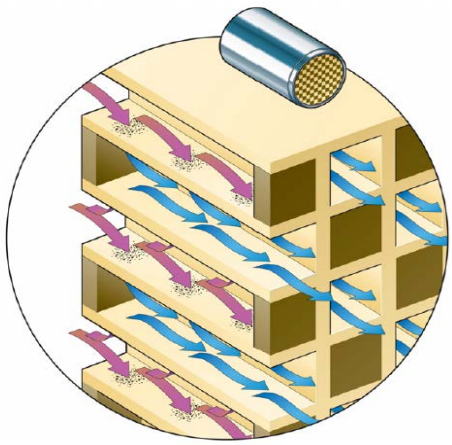

Figure 1.1 Porous walls of a DPF [3].

However, as the PM or soot is retained by the filter, the filter passageway increasingly becomes more restrictive resulting in elevated back pressure in the exhaust. This furthers results in lower fuel efficiency for the engines since the pistons have to exert more pressure to purge the exhaust gas. One effective way to address this problem is to burn the soot load in the DPF periodically either by injecting more fuel in the engine or by a separate combustor upstream of the DPF with the aid of a diesel oxidation catalyst (DOC). The latter which is known as active regeneration of DPF is more efficient and is commonly used for DPF. Here a fuel doser is used to raise the exhaust gas temperature to

burn off the soot load in DPF. The timing and amount of fuel dosing is critical in ensuring optimal performance of DPF functions. Current commercially available DPF particulate matter detection methods are mostly based on pressure differences. This sensor is suitable for meeting the stricter environment requirements of Figure 1.2 but this particular sensor doesn't have proper accuracy to reduce the fuel penalty [4].

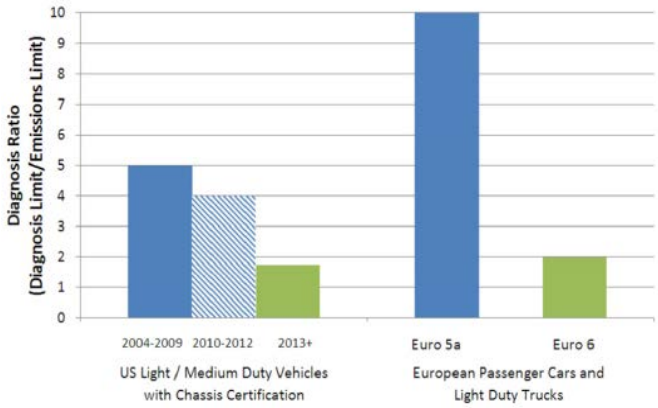

Figure 1.2 DPF diagnosis regulatory requirements [5].

The performance efficiency of a DPF with active regeneration is largely dependent on the accuracy of soot load estimation. Current soot load estimation is based on differential pressure measurement across the DPF whose accuracy can vary up to ±50% from the true soot load [6]. As a result, fuel dosing for active regeneration may not be optimal. It has been shown that fuel penalty caused by regeneration (2.2% to 5.3 %) is more than fuel penalty due to backpressure (1.5% to 2.0 %) [7]. Accurate soot load knowledge is also necessary if one wants to rule out possible overheating of the DPF caused by exothermic soot oxidation. Because if DPF is allowed to accumulate too much particulate matter, the large amount of heat released upon regeneration cannot effectively

be dissipated, resulting filter damage such as by the formation of cracks or regions which may be locally melted.

The knowledge of the tomography of DPF is a very important to minimize the impact of fuel consumption and avoid damaging the filter and other after treatment systems. In this paper we present a novel instantaneous soot load sensor based on electrical capacitance that can improve the soot load estimation. This sensor can be used in the feedback loop to improve the soot load estimation allowing for correct amount of fuel injection upstream of diesel oxidation catalyst (DOC) and thus potentially improving the overall DPF performance. For this reason we have explored the designing, building, and implementing a feedback control system for an actively regenerated DPF based on real time electrical capacitance soot load sensor feedback and presented it here for the first time.

1.2 Literature Review

The paper by Rose et al describes soot mass estimation using pressure drop signal combined with other parameters [8]. This team basically focuses on the real world accuracy during highly transient operation. In this study two different approaches were evaluated. The issues regarding pressure drop measurement is pressure drop response of the filter depends on several factors, which are

1. Inlet effect and flow profile
2. Friction along inlet
3. Loses due to the resistance to flow through the wall
4. Friction along outlet

5. Expansion at outlet.

Only factors number 2 and 3 are affected by soot, on the other hand other factors do not depend on soot. DPF materials exhibit a nonlinear initial increase in pressure drop with PM load due to deep bed filtration. Though deep bed filtration is quite common phenomenon for a DPF soot deposition, in this paper this phenomenon been neglected and instead a typical method to minimize the deep bed filtration has been assumed. Nonetheless, the geometric intricacies are also going to be involved in pressure drop. If the DPF designed in such a way so the pressure drop gets a shallow slope then the detection of pressure drop will be more complex. Soot detection using pressure drop may be accepted for a while but it will not be sufficient to meet the newer and stricter regulations.

Differential pressure detection has few limitations so researchers are pursuing other means for detecting the soot deposition. Husted et al in their paper “sensing particulate matter for on board diagnosis of particulate filters” explore the possibilities of soot measurement using particulate material sensor placed at the exhaust stream [5]. With the deposition of the soot along the surface of the sensor the electrical conductivity will increase and is measured as part of an electrical circuit. To use this particular method the sensor has to be very robust in design. Because the placement of sensor will be directly inside the exhaust stream, so it has to withstand the exposure of urea, water impingement, poison, ash, acid, and very high temperature like 900^{o}C. Apart from these alien objects the sensor element must be above the dew point temperature to reduce the response delay. Though by using conventional contaminant protection coating on the sensor material

contamination problem can be eliminated but then soot have to use a torturous path to reach the sensor itself.

Fischerauer et al used current microwave technology; which mostly used in typical phones, to measure the soot inside DPF [3]. This approach is based on the interaction of electromagnetic fields or waves at microwave frequencies with the DPF. Researchers assume that the addition of soot in a dielectric medium will influence its permittivity and conductivity, which should be observable via resonance frequency shift or via changes in the attenuation of the resonance peaks. This is basically cavity perturbation method. One set of microwave generator and receiver is required for the detection and then from the difference of frequency dependent scattering matrix soot deposition amount gets detected. The main concern regarding this measuring method is about cost and robustness. Microwave generator integrated circuit is still not very cheap and robustness may also be an issue with the cavity feeds.

Sappok et al is working on another cutting edge method of filter soot sensing using radio frequency based sensor [4]. In this method two antennas will be installed on either side of a DPF filter. A pair of coaxial cable connects the pair of antennas with an electronic control device. The Radio Frequency signal characteristics will be influenced by the dielectric property of the material through it propagates. Signal amplitude and transmitted power is a function of the losses within the material through which the wave travels. With the increase of DPF soot deposition. Dielectric properties also changes which affect the RF signal directly. The RF sensor response is insensitive to flow variation unlike pressure drop. Though RF based sensors shows suitable results in both steady state and transient condition, it is still very hard to generate a tomographic image

of DPF using RF sensor. Without the tomographic image DPF axial loading condition will not be visible, Still more research is going on in this field. GE shared a product named Accusolve Diesel particulate filter soot sensor in the market.

Strzelec et al from Oak ridge national laboratory are researching on nondestructive neutron computed tomography measurement of DPF to measure soot [9]. Past studies of soot loading have been done using transmission electron microscopy imaging and later nondestructive x-ray imaging. First one is destructive method and the former one provided images with very low contrast. On the other hand neutron imaging is a nondestructive method and can provide results with good resolution. Basic principle of this method is whenever a neutron beam is passing through matter then there will a attenuation of the beam caused by absorption and scattering of material. By measuring the intensity of the attenuated signal material properties can be detected. Using this method quantification of soot loading can be done but using the whole neutron beam setup for real time soot measurement in an automotive engine or a power generator engine is still very expensive.

All the previously mentioned methods do have some limitation for soot load measurement. After studying through all those papers it is obvious that for soot load measurement sensor has to be accurate, robust, and cost effective. Authors of this work have conducted several studies for an ideal soot load sensor using electrical capacitance tomography which is shown to be more accurate, robust, and inexpensive compared to the existing sensors.

2. MODELING OF ELECTRICAL CAPACITANCE TOMOGRAPHY

2.1 Permittivity Model

For this paper modelling of a complete ECT Diesel particulate filter soot measurement system requires three subsystems, Electrical capacitance tomography sensor, Diesel particulate filter model and Data acquisition system model. Designing these three subsystem models are a compromise between the achievability of real world scenarios and the possibility of obtaining such results from the least usage of resources i.e. the usage of computational time, usage of technical know-how of engineers as well as the computational power required.

Two parallel plates of a conducting material separated by an air gap have been connected through a switch and a resistor to a signal generator. The instant the switch is closed; electrons are drawn from the upper plate through the resistor to the positive terminal of the signal generator. This action creates a net positive charge on the top plate. Electrons are being repelled by the negative terminal through the lower conductor to the bottom plate at the same rate they are being drawn to the positive terminal. This transfer of electrons continues until the potential difference across the parallel plates is exactly equal to the battery voltage. This element is called a capacitor.

If a potential difference of V volts is applied across two plates separated by a distance of d, the electric field strength between the plates is determined by E.

$$E = V/d \quad (1)$$

The ratio of the flux density to the electric field intensity in the dielectric is called the permittivity of the dielectric [10].

$$\varepsilon = D/E \quad (2)$$

For a vacuum, the value of Ɛ (denoted by Ɛo) is $\varepsilon_o = 8.854 \times 10^{-12}$ F/m. The ratio of the permittivity of any dielectric to that of a vacuum is called the relative permittivity, $Ɛ_r$. It simply compares the permittivity of the dielectric to that of air.

$$\varepsilon_r = \varepsilon/\varepsilon_o \quad (3)$$

If the charge Q is large enough then flux density D can be written as

$$D = Q/A$$

$$\varepsilon = \frac{D}{E} = \frac{Q/A}{V/d} = Qd/VA$$

Again $C = Q/V$

Therefore $\varepsilon = Cd/A$

$$C = \varepsilon A/d$$

Or, $C = \varepsilon_o \varepsilon_r A/d \quad (4)$

Based on the above mentioned principle and equation (4), Electrical capacitance tomography (ECT) system been established. The capacitance measured depends on the relative permittivity of the materials between the electrodes. Their relation can be linear or nonlinear in nature. It depends on the permittivity models used to characterize the way in which the contents occur. The various permittivity models used are the series model, parallel model, and Maxwell's model.

Suppose one substance of relative permittivity ε_r and air mixed together. That substance occupy x of the total space between two electrodes. The effective permittivity of the mixture and their dependence on capacitance for various models are explained in the following sections.

2.1.1 Series Permittivity model

Two components with relative permittivity ε_r and ε_o in the pipe lie on top of one another, the effective capacitance can be considered as two capacitances connected in series. This is illustrated in Figure 2.1. In this case, the capacitance and permittivity are related in a nonlinear fashion. Mostly for primary experiments series permittivity model or parallel permittivity model has been considered in this work. The effective permittivity denoted by ε_s and overall capacitance denoted by C_s is given respectively in equation (5) and equation (6) [11].

$$\varepsilon_s = \frac{\varepsilon_r \varepsilon_o x(1-x)}{1-x(\varepsilon_r - 1)} \tag{5}$$

$$C_s = {A\varepsilon_s}/{d} \tag{6}$$

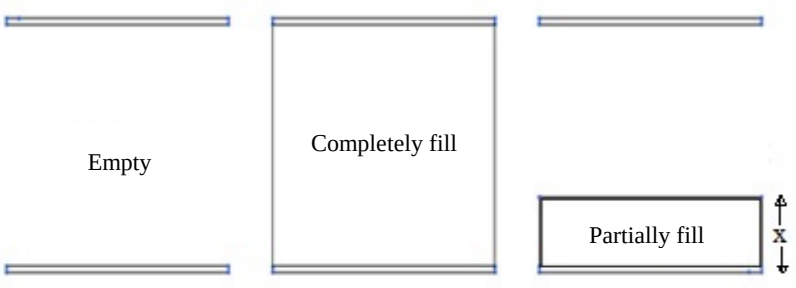

Figure 2.1 Empty, completely filled and partially filled.

2.1.2 Parallel Permittivity Model

Two components with relative permittivity ε_r and ε_o in the pipe are appeared as discrete band and appear side by side, their effective capacitance can be considered as two capacitances connected in parallel. This is illustrated in Figure 2.2. In this case, the capacitance and permittivity are related linearly. The effective permittivity and overall capacitance is given respectively in equation (7) and equation (8). [11]

$$\varepsilon_p = \varepsilon_o[1 + x(\varepsilon_r - 1)] \tag{7}$$

$$C_p = {A\varepsilon_p}/{d} \tag{8}$$

Figure 2.2 Empty, completely filled and partially filled.

2.1.3 Maxwell Garnett Permittivity Model

The generalized Maxwell Garnett mixing formula for multiphase mixtures with randomly oriented ellipsoidal inclusions [12]. In this model two materials of relative permittivity ε_i and ε_b are mixed randomly like Figure 2.3, then the effective permittivity become ε_m. here f_i is the volume fraction occupied by the inclusions of the i-th type, N_{ik} are the depolarization factors of the i-th type of inclusions.

$$\varepsilon_m = \varepsilon_b + \frac{\frac{1}{3}\sum_{i=1}^{n} f_i(\varepsilon_i - \varepsilon_b)\sum_{k=3}^{3}\frac{\varepsilon_b}{\varepsilon_b + N_{ik}(\varepsilon_i - \varepsilon_b)}}{1 - \frac{1}{3}\sum_{i=1}^{n} f_i(\varepsilon_i - \varepsilon_b)\sum_{k=3}^{3}\frac{N_{ik}}{\varepsilon_b + N_{ik}(\varepsilon_i - \varepsilon_b)}} \tag{9}$$

$$C_s = A\varepsilon_s / d \tag{10}$$

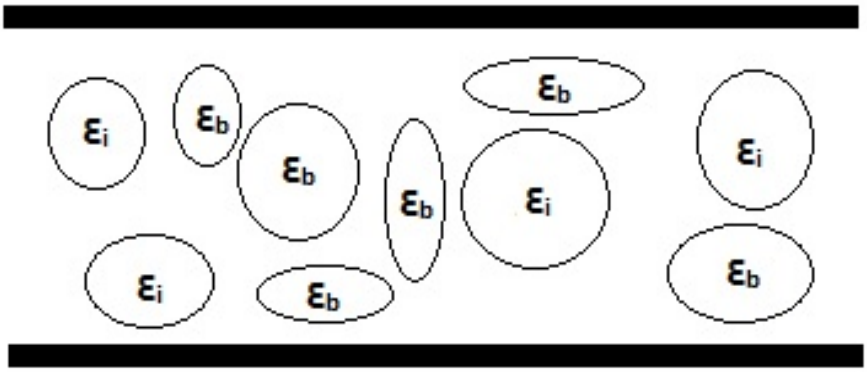

Figure 2.3 Multiphase mixtures inside capacitor.

2.2 Electrical Capacitance Tomography Measurement Principle

Electrical capacitance tomography (ECT) is used to obtain information about the spatial distribution of a mixture of dielectric materials inside a vessel, by measuring the electrical capacitances between sets of electrodes placed around its periphery and

converting these measurements into an image or graph showing the distribution of permittivity [13]. The images are approximate and of relatively low resolution, but they can be generated at relatively high speeds.

ECT can be used with any arbitrary mixture of different non-conducting dielectric materials such as plastics, hydrocarbons, sand or glass. However, an important application of ECT is viewing and measuring the spatial distribution of a mixture of two different dielectric materials (a two-phase mixture), as in this case, the concentration distribution of the two components over the cross-section of the vessel can be obtained from the permittivity distribution.

An ECT system consists of a capacitance sensor, Capacitance Measurement Unit (CMU) and a control computer. For imaging a single vessel type with a fixed cross-section and with a fixed electrode configuration, the measurement circuitry can be integrated into the sensor and the measurement circuits can be connected directly to the sensor electrodes. This simplifies the measurement of inter-electrode capacitances and is potentially a good design solution for standardized industrial sensors.

However, most current applications for ECT are in the research sector, where it is preferable to have a standard capacitance measuring unit which can be used with a wide range of sensors. In this case, screened cables connect the sensor to the measurement circuitry, which must be able to measure very small inter-electrode capacitances, of the order of 10-15 F (1 fF), in the presence of much larger capacitances to earth of the order of 200,000 fF (mainly due to the screened cables)[14]. A diagram of a basic ECT system of this type is shown in Figure 2.4.

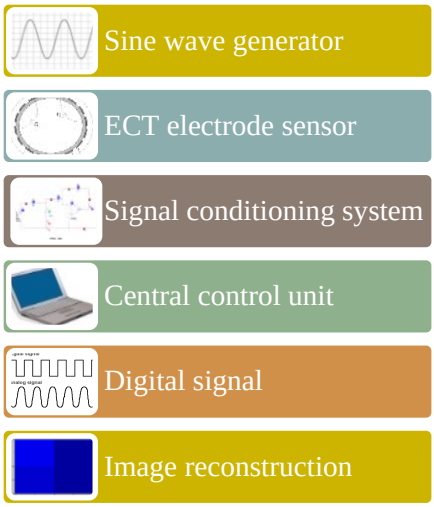

Figure 2.4 Electrical Capacitance Tomography systems flow chart.

ECT system is a set of capacitor plates placed around a pipe or any other vessel. A source voltage is applied between one electrode (the source electrode) and ground and the resulting currents flow between the source electrode and the remaining (detector) electrodes to ground are measured. These currents are directly proportional to the capacitances between the source and detector electrodes. The set of capacitance measurements made.

In ECT a complete set of measurement projections is made by exciting each electrode in turn as a source electrode and measuring the currents which flow into the remaining detector electrodes. So for an 8-electrode sensor, as shown in Figure 2.5 there will be 8 x 7 = 56 possible capacitance measurements. However, as half of these will be reciprocal measurements (the same capacitance should be measured by exciting electrode 1 as a source and measuring the current into electrode 2 as is obtained by exciting electrode 2 as a source and measuring the current into electrode 1 etc.), there will only be

28 unique capacitance measurements for a complete set of projections. In general for a sensor with E electrodes, there will be E*(E-1)/2 unique capacitance measurements.

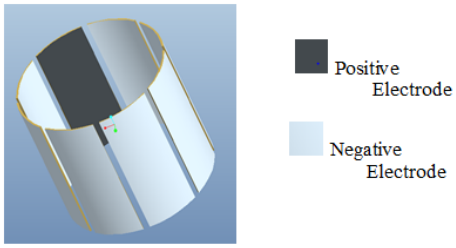

Figure 2.5 Capacitance measurement principles.

The set of measured inter-electrode capacitance values and subsequently obtained permittivity's are normalized to construct the permittivity images.

$$\text{Capacitance normalize } C_n = \frac{C_i - C_i(emp)}{C_i(full) - C_i(emp)} \quad 0 < C_n < 1.$$

$$\text{Permittivity normalize } K_n = \frac{K_i - K_i(emp)}{K_i(full) - K_i(emp)} \quad 0 < K_n < 1.$$

The normalized values are then projected into a square pixel grid where the pixel values are similarly normalized to lie between 0 to1. The image formed is not an exact solution but an approximate solution.

2.3 Tomographic Image Formation

The permittivity image or tomographic images are mapped onto a square pixel grid. The complete set of a measured inter-electrode capacitance values is required to reconstruct one permittivity distribution image. Figure 2.6 shows a 16x16 square pixel grid used to display the permittivity distribution image of a 4-electrode sensor having circular intersection of Diesel particulate filter.

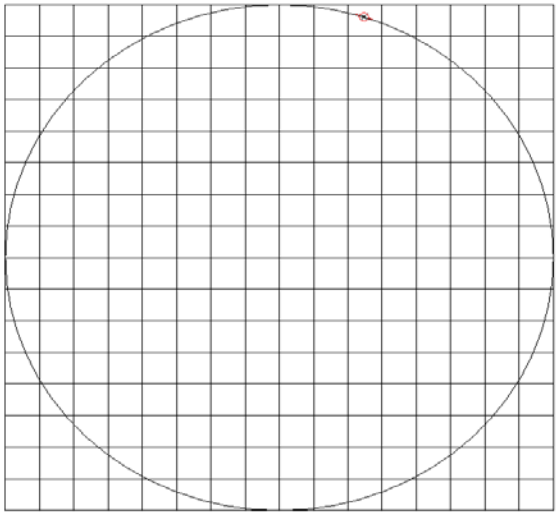

Figure 2.6 Square pixel grid.

From this (16x16) square pixel grid containing 256 pixels, only 224 are needed to construct the cross sectional image of the DPF and remaining pixels are not required and hence neglected.

The field lines between two plates are curved and to suit the requirement these lines can be approximated. A proper sensitivity map, purpose of which is to aid in selecting the proper pixel that individually contributes to the capacitance changes, have to be developed for visualizing the electric field established between two electrodes when one of them is excited.

A simple procedure for reconstructing an image of an unknown permittivity distribution inside the sensor from the capacitance measurements is the Linear Back Projection (LBP) algorithm [15]. Although its reconstruction accuracy is not very good, LBP has the advantage of being quite fast, in practice requiring only the multiplication of a fixed reconstruction matrix times the vector of measurements.

Let us consider an x-electrode sensor, from which N number of voltage data has been recorded, and square pixel grid pixel number is M. A grey level K(M) for each pixel has been calculated by the basic LBP formula. [16].

$$K_1 = S_{a1} \times C_1 . + S_{a2} \times C_2 + S_{a3} \times C_3 + S_{a4} \times C_4 + S_{a5} \times C_5 + ... + S_{aN} \times C_N$$

$$K_2 = S_{b1} \times C_1 . + S_{b2} \times C_2 + S_{b3} \times C_3 + S_{b4} \times C_4 + S_{b5} \times C_5 + ... + S_{bN} \times C_N$$

….

….

$$K_M = S_{M1} \times C_1 . + S_{M3} \times C_3 + S_{M3} \times C_3 + S_{M4} \times C_4 + S_{M5} \times C_5 + ... + S_{MN} \times C_N$$

The relationships presented above between capacitance permittivity distributions can be written in a normalized form as:

$$\begin{matrix} K_1 \\ K_2 \\ K_3 \\ . \\ K_M \end{matrix} = \begin{matrix} S_{a1} & S_{a2} & S_{a3} & . & S_{aN} \\ S_{b1} & S_{b2} & S_{b3} & . & S_{bN} \\ S_{c1} & S_{c3} & S_{c3} & . & S_{cN} \\ . & . & . & . & . \\ S_{M1} & S_{M2} & S_{M3} & . & S_{MN} \end{matrix} \times \begin{matrix} C_1 \\ C_2 \\ C_3 \\ . \\ C_N \end{matrix}$$

$$K = SC \tag{11}$$

C = N X 1 matrix containing the normalized electrode-pair capacitances Cm (in the nominal range 0 to 1).

K = M X 1 matrix containing the normalized pixel permittivity's (in the nominal range 0 to 1) N is the number of pixels representing the sensor cross-section

S = M X N matrix containing the set of sensitivity matrices for each electrode-pair. This sensitivity map can be defined as

$$S_{Mi} = \frac{C_i - C_i(emp)}{C_i(full) - C_i(emp)} \; for i = 1...N \; .$$

The sensitivity matrix describes how the measured capacitance between any combinations of electrodes changes when a change is made to the dielectric constant of a single pixel inside the sensor. Here $C_i(emp)$ is the capacitance voltage when DPF is completely empty and $C_i(full)$ is the capacitance voltage when DPF is completely full. The properties of the capacitance sensor are measured or calculated initially to produce a sensor sensitivity matrix for the case when the sensor is empty. Sensitivity matrix is a composed of a set of sub- matrices (or maps) whose elements correspond to the individual pixels in a rectangular grid which is used to define the sensor cross-section. The sensor is normally calibrated at each end of the range of permittivity to be measured by filling the sensor with the lower permittivity material initially and measuring all of the individual inter-electrode capacitances. This operation is then repeated using the higher permittivity material. The data obtained during the calibration procedure is used to set up the measurement parameters for each measuring channel and is stored in a calibration data file.

In principle, once the set of inter-electrode capacitances C has been measured, the permittivity distribution K can be obtained from these measurements using equation (11).

Direct contributions of pixels to the measured capacitance between any specific electrode-pair is not be specified, but it can be shown from the sensitivity matrix S that certain pixels have more effect than others on this capacitance. Consequently, component values allocated to each pixel proportional to the product of the electrode-pair capacitance and the pixel sensitivity coefficient for this electrode-pair. Based on this

approximation the LBP algorithm uses the sensitivity matrix, S an approximate matrix which has the dimensions (M x N).

This process is repeated for each electrode-pair capacitance in turn and the component values obtained for each pixel are summed for the complete range of electric pairs.

3. SIMULATION RESULT

Previous Studies regarding diesel soot dielectric properties has shown that in microwave range dielectric constant of soot has dependency on the soot layer thickness which is captured in Figure 3.1.

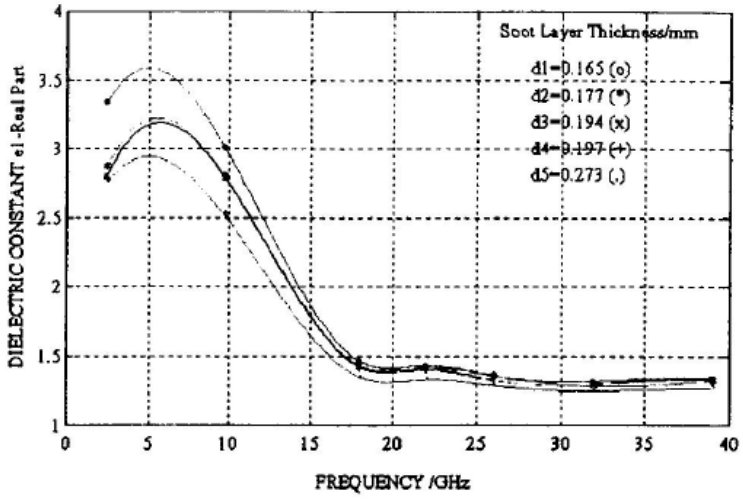

Figure 3.1 Real part of dielectric constant and soot layer thickness [17].

In this model Series Permittivity Model has been chosen to calculate the effective permittivity of soot and air mixture.

$$\varepsilon_s = \frac{\varepsilon_r \varepsilon_o x(1-x)}{1-x(\varepsilon_r - 1)}$$

$$C_s = A\varepsilon_s / d$$

In the model the length of DPF set at 6 inch, so the length of the capacitor plate will be 6 inch and for 4 capacitor plate ECT sensor the width of the capacitor plate will be 4.71 inch (approx.) and maximum distance between two plates will be 5.6 inch. So

$$\varepsilon_s = \frac{5 \times 8.854 \times 10^{-12} \times (1-2)}{1-2(5-1)} = 1.2649 \times 10^{-11}$$

$$C_s = 6 \times 4.72 \times 1.2649 \times 10^{-11} / 5.6 = 63.8301\,\text{pF} \qquad (12)$$

A model of the soot detection system has been designed in PSpice to check the detection voltage in Figure 3.2 and output result has been shown in Figure 3.3.

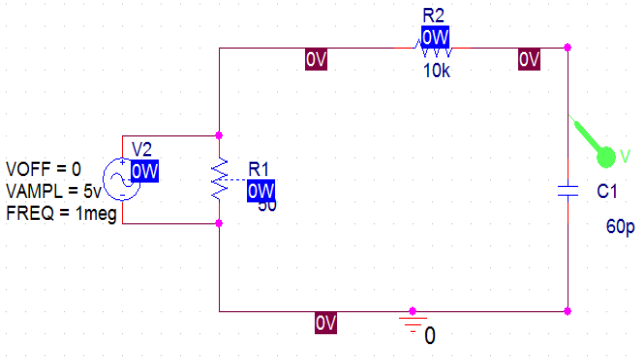

Figure 3.2 5V AC input in 60pF capacitor circuit.

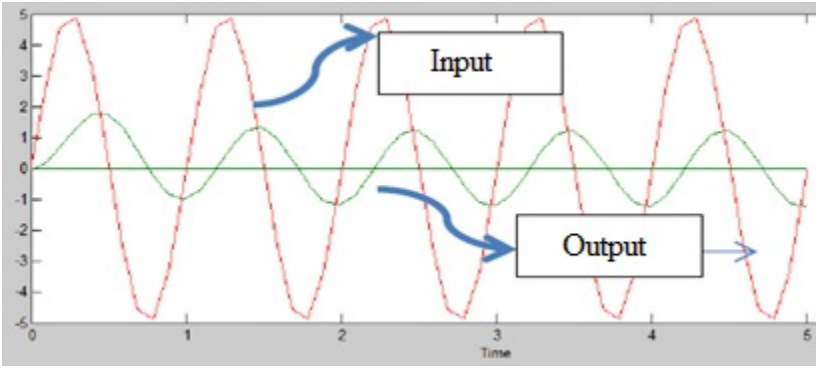

Figure 3.3 output Voltage 1.6-1.7v for 5us.

An Ac 5 volt 1 MHz has been supplied for 3 different types of capacitance values 60 pF, 90 and 130pF and output voltage has been checked. Results are shown in Table 3.1 and plot of Figure 3.3. Capacitance values are calculated from experimental electrode model and Equation 12.

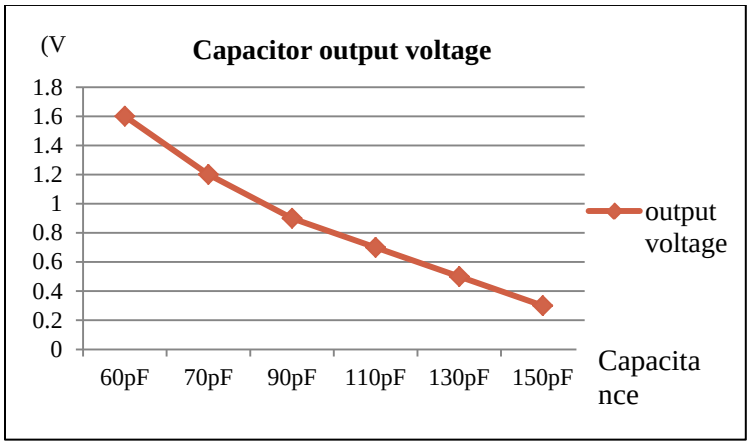

Figure 3.4 Relationships between output voltage and capacitance.

Table 3.1 Output voltages for different capacitance values

Input Voltage	Capacitance	Output Voltage
5 VAC	60pF	1.6-1.7
5 VAC	70pF	1.2-1.3
5 VAC	90pF	0.9-1.0
5 VAC	110pF	0.7-0.8
5 VAC	130pF	0.5-0.6
5 VAC	150pF	0.3-0.4

Above simulation results showed that even a very small amount of soot deposition causes variation on the output voltage. Applying these capacitance values and voltage

values in linear back projection algorithm will help to build the tomographic information of a DPF.

After data acquisition device collects all the capacitance values from capacitor voltage, these values needed to be normalize. Assume a 4 capacitor plate used in an ECT system just like Figure 3.5(a). The final tomography image will be constructed in a 2*2 pixel as following in Figure 3.6.

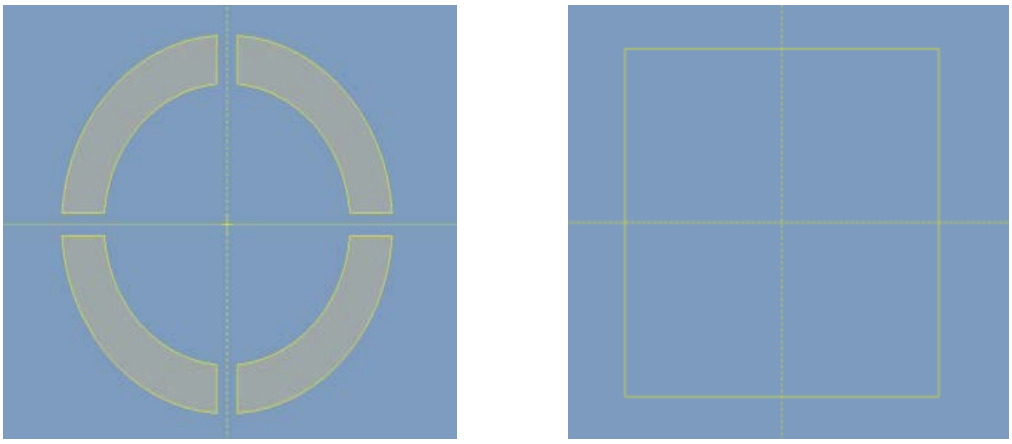

(a) (b)

Figure 3.5 Four capacitor plates positions in ECT and 2*2 pixel grid.

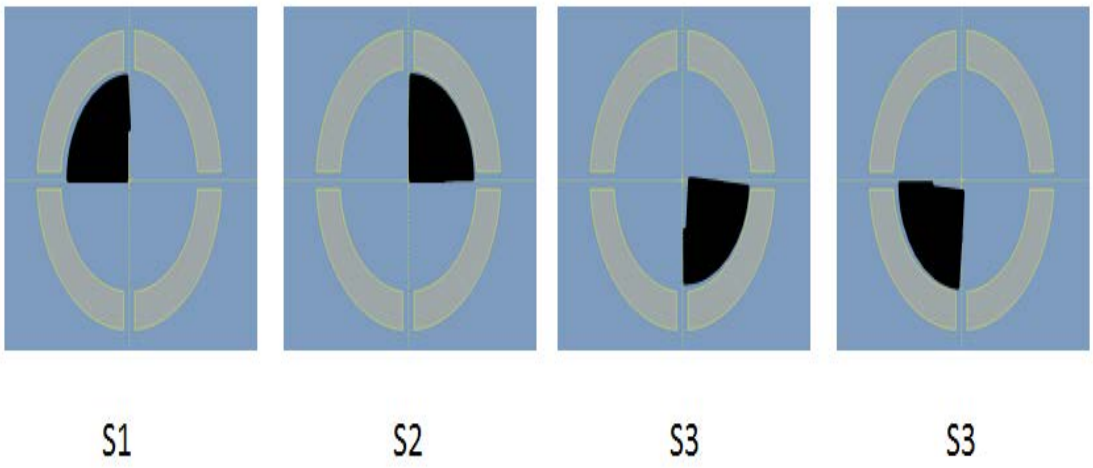

Figure 3.6 Sensitivity matrixes.

Now in a real time scenario if particulate materials accumulates inside of a DPF in the following manner like Figure 3.7(a) then the normalize values of ECT system outputs will be C = [0.6; 0.2; 1; 0; 0.2; 0.6] with the tomographic image like Figure 3.7(b).

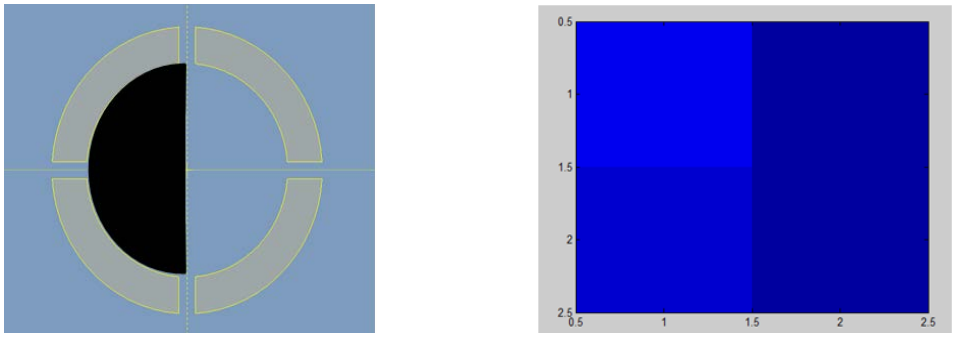

(a) (b)

Figure 3.7 Particulate deposition and Tomographic image.

4. EXPERIMENTAL SETUP

The experimentation of soot measuring system using ECT is going on in an experimental model of DPF made of Nylon 66, unreinforced, and flame retardant [18]. This Nylon 66 has very close dielectric properties of conventional DPF made from cordierite which has dielectric constant of 4.7(approx.) in 1MHz [19].

The DPF outer shell wall is conductive so the ECT system electrode has to be placed inside of the DPF wall. In that case the components of capacitance due to the electric field inside the sensor will always increase in proportion to the material permittivity when a higher permittivity material is introduced inside the sensor.

The internal temperature of DPF will be highest when the regeneration of soot is taking place. Regeneration is a process of soot removal from the DPF and there are two different approaches existed one is active and another is passive. Active systems use extra fuel, whether through burning to heat the DPF, or providing extra power to the DPF's electrical system. This process required 600°C to burn Diesel particulate matter. This temperature can be reduced to somewhere in the range of 350°C to 450°C by use of a fuel borne catalyst [3]. There is a more effective way to burn soot at lower temperature brought by Johnson Matthey’s novel two-component design [3]. In this novel approach the catalyst is positioned before the filter to convert NO into NO2. Then The NO2 oxidizes the soot which is collected on the filter to regenerate the filter at a much lower

temperature than is normally required. In fact, the CRT-continuously regenerating technology enables the filter to be regenerated at a temperature that is 20% lower than other filters on the market. By using this approach the soot burning temperature can be reduced up to 240°C. So whatever material we are using as ECT electrode it has to be able to withstand a versatile range of temperature. The properties that led us to choose copper as ECT electrode are [20]

1) Melting point at 1357°K or 1084°C
2) Do not reacted with water
3) Resistivity = $1.68\times10^{-8}(\Omega\bullet m)$ at 20 °C
4) Conductivity = $5.96\times10^{7}\ (s/m)$ at 20 °C
5) Temperature coefficient = 0.003862(K^{-1})
6) Copper resists corrosion from moisture, humidity and industrial pollution
7) However products from other carrion like oxide, chloride and sulfide are conductive.

Due to very low temperature coefficient of copper the change of conductivity with the change of temperature will be very low. If the assumption made that the temperature change inside of DPF is linear then relationship between resistivity and temperature will be

$$\rho(T) = \rho_o[1 + \alpha(T - T_o)]$$

$$\rho(T) = 3.489\times10^{-8}(\Omega\bullet m)$$

Figure 4.1 shows an isometric view of the experimental setup with 8 capacitance electrodes and DPF model of 152mm (6 in) length with 130mm (5 in) diameter. There is a trade-off has to be done to choose the number of electrode. Higher number of electrode means complicated and expensive data acquisition hardware, smaller capacitance to be measured; slower data acquisition as we can see from Table 2 and currently 8-12 numbers of electrodes are commonly used in an ECT sensor. These 8 electrodes have to be placed around the DPF.

Table 4.1 Number of electrodes vs number of independent measurement [21]

Number of electrodes	**Independent Measurement**	**Typical speed**
6	15	400 [22]
8	28	200 [23]
12	66	100[24]
16	120	50 [25]

A common practice for the length of the ECT sensor is diameter has to be smaller than the length to avoid serious fringe effect [13]. So if the DPF diameter size is larger than the length then fringe effect cannot be ignored. For experimental purpose in this paper the filter model used with typical dimensions of 130mm (5in.) diameter and 152mm (6in.) length [13]. For the experimental setup length of the electrode is larger than the diameter of ECT system. For this experimental setup fringe effect completely ignored.

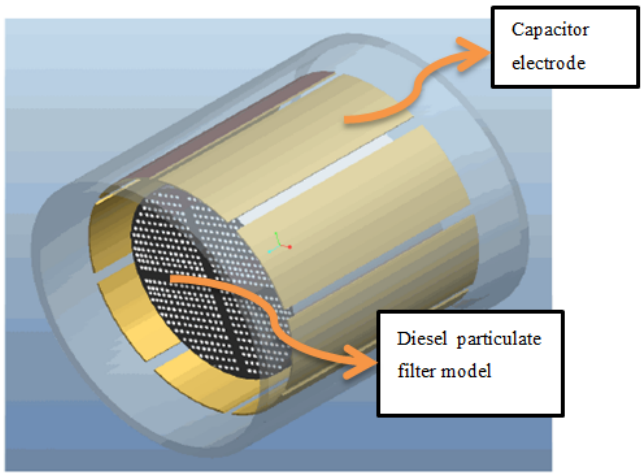

Figure 4.1 Isometric View of Setup.

The test bench is equipped with an automatic National instruments data acquisition system NI DAQ-6008 for capturing the capacitance values. Research team is using dry sand as a replacement of soot to verify the approach of using Electrical capacitance tomography to soot detection. Properties of dry sand are following [26]

1) Density 1.60 - 1.70 g/cc
2) Electrical Resistivity 1000 - 100000 ohm-cm
3) Specific Heat Capacity 0.753 - 0.799 J/g-°C
4) Thermal Conductivity 0.270 - 0.340 W/m-K

Two different methods of sand distribution have been considered while conducting the experiments. In concentrated distribution the assumption is at first sand start accumulation near to one particular electrode, and later filled up the whole filter. Voltage applied on the RC circuit is 4v with 100 kHz frequency, approximation of frequency done from previous studies and experiments [27], which resulted output

voltage plot just as Figure 4.2. On the other hand in uniform distribution the assumption is the sand distributed equally through the whole filter resulted output voltage plot like Figure 4.3. Data acquisition hardware senses the change of sand accumulation by the changes of the capacitance plate voltages. Voltage signals were processed in LABVIEW and Figure 4.2 and Figure 4.3 are depicting the fact that with the increase of sand accumulation the voltage is also changing.

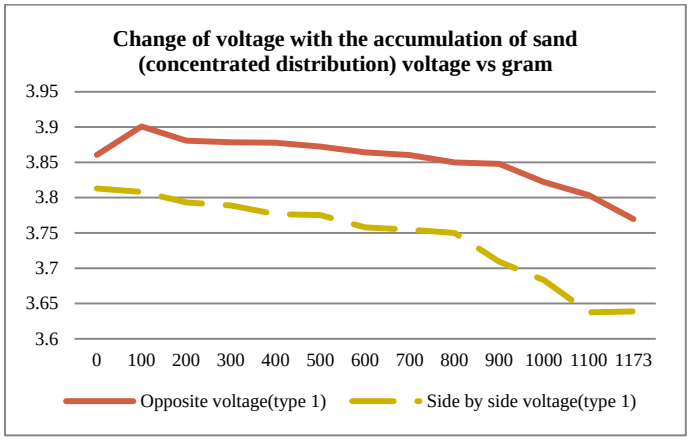

Figure 4.2 Voltage Change with the accumulation of sand (concentrated distribution).

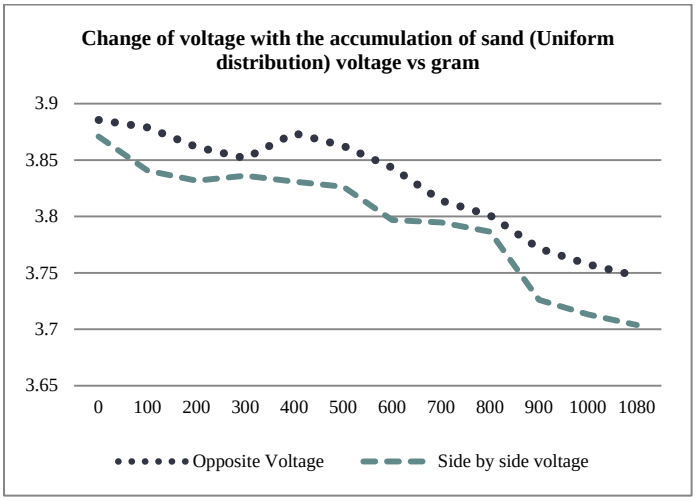

Figure 4.3 Voltage Change with the accumulation of sand (Uniform distribution).

From Figure 4.2 and 4.3 it is visible that with the change of soot deposition output capacitor voltage also occurs in a detectable range. To clarify the result repeatability another graph has been implemented in Figure 4.4. This figure has depicted all the experimental results for Voltage V_{AB} change vs soot deposition inside DPF from 10% to 100%. From Figure 4.4 the irregularities in linearity of Figure 4.2 and 4.3 are conceivable.

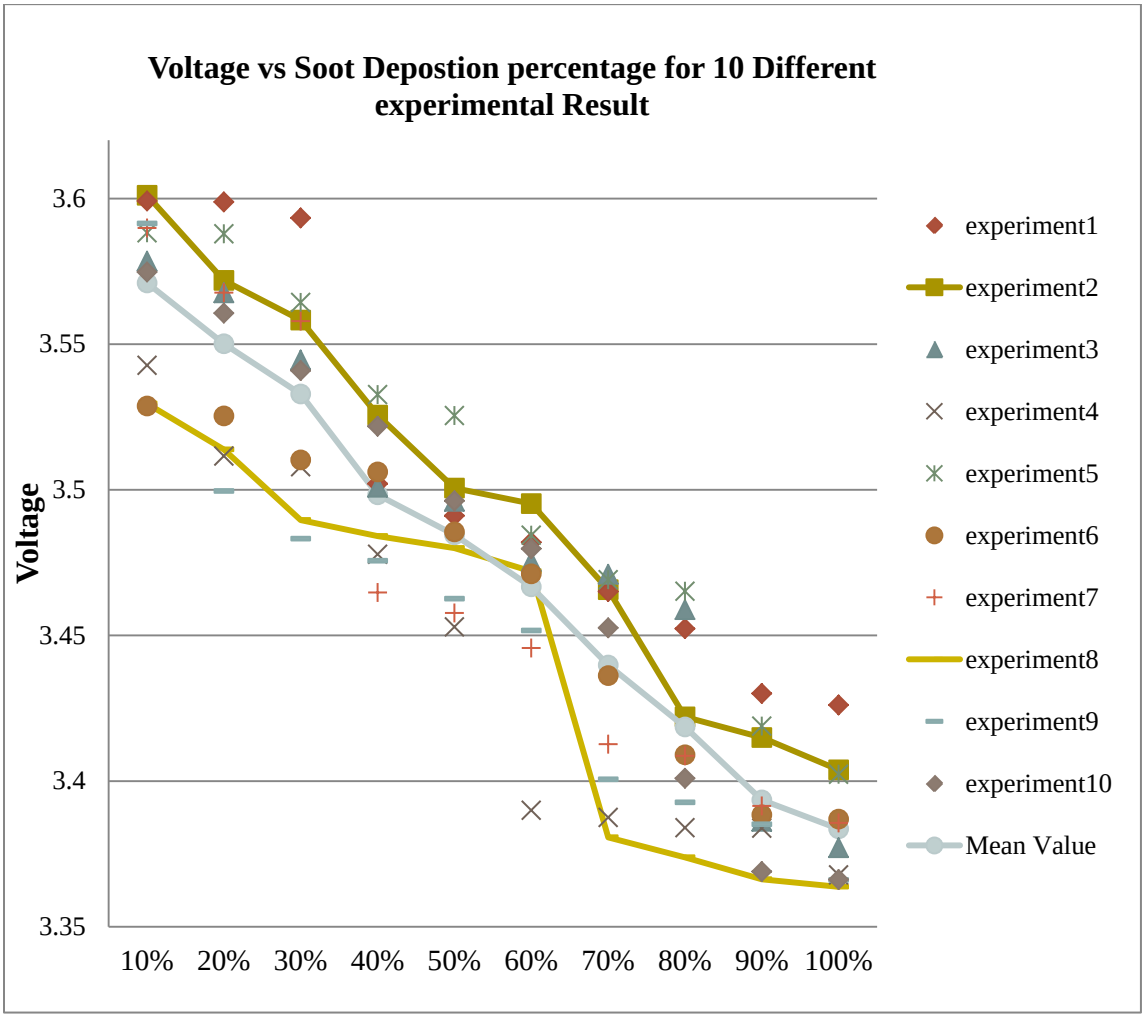

Figure 4.4 Variability in experimental results.

Above figure shows the complete experimental setup to identify the relationship between output voltage and amount of accumulated material.

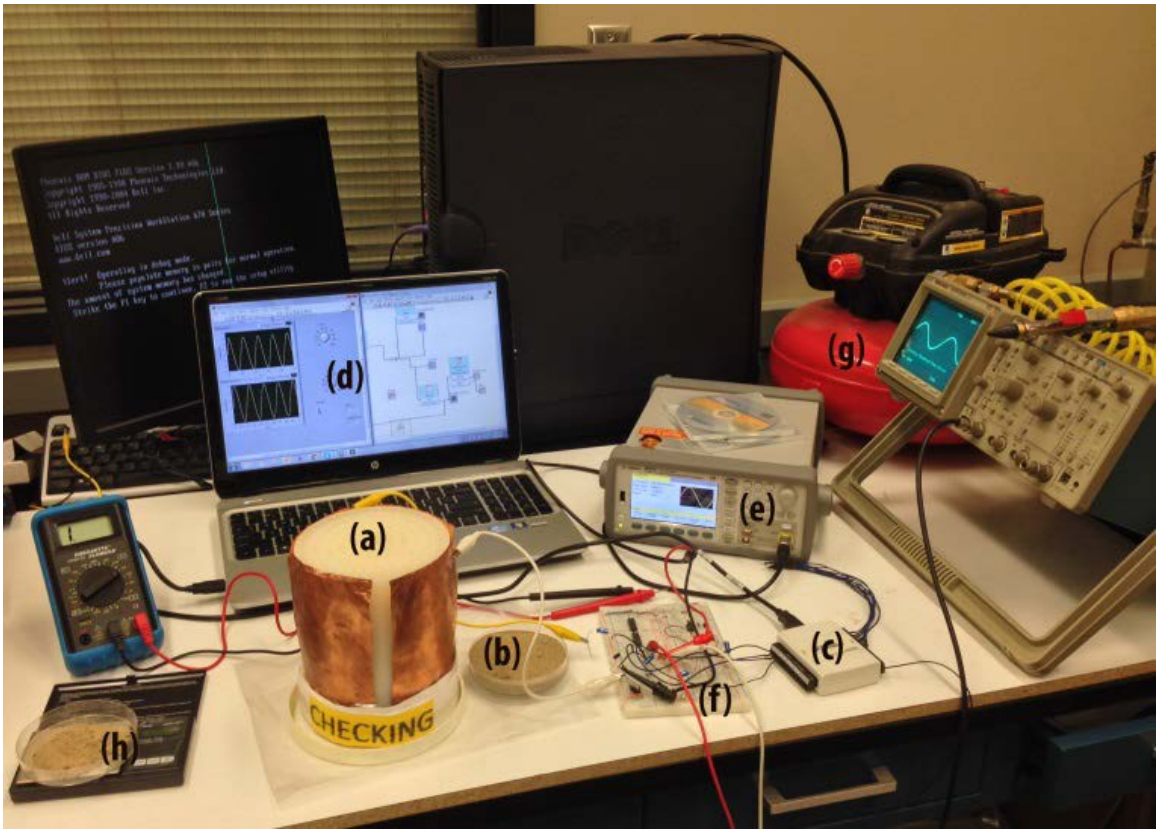

Figure 4.5 Experimental setup; (a) Filter model, (b) Sand as soot replacement, (c) NI DAQ, (d) Data acquisition program, (e) Signal generator, (f) Data acquisition circuit, (g) Blower, (h) Material weighing.

5. EXPERIMENTAL RESULTS

5.1 Rule Based Tomographic Image Generation

A completing set of experimentation has been conducted on the test bench using sand (density 1.6-1.9 g/cm3) as soot model, Nylon 66 as DPF model and four copper electrodes. Electrodes will be arranged like Figure 5.1.

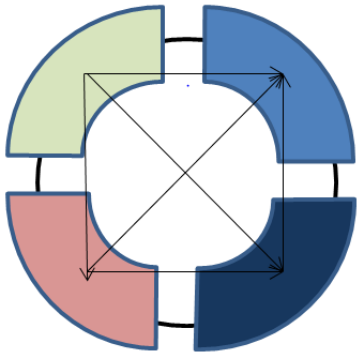

Figure 5.1 Four electrode arrangement.

Sand has been poured into the grooves of DPF in a uniform fashion and simultaneously capacitance voltages between A-B VAB, A-C VAC, A-D VAD, B-C VBC, B-D VBD and C-D VCD has been measured using the NI DAQ-6008 device and LABVIEW [28].

Now to prepare detection image we need to consider a 2 by 2 pixel matrix. To assign the value of each pixel we need to normalize the capacitance voltage value. Every pixel will have certain normalize capacitance voltage values like Figure 5.2.

Table 5.1 Experimental capacitance data set

Weight of sand	**Total**	**A-B (V_{AB})**	**A-C (V_{AC})**	**A-D**	**B-C**	**B-D**	**C-D**
0	0	3.946	3.998	3.902	3.857	3.963	3.823
100	100	3.983	3.961	3.897	3.806	3.902	3.851
100	200	3.972	3.957	3.889	3.904	3.894	3.802
100	300	3.966	3.955	3.878	3.838	3.876	3.828
100	400	3.925	3.942	3.878	3.826	3.867	3.822
100	500	3.942	3.941	3.867	3.821	3.856	3.823
100	600	3.929	3.91	3.856	3.866	3.87	3.813
100	700	3.905	3.904	3.823	3.848	3.858	3.733
100	800	3.867	3.928	3.849	3.838	3.878	3.722
100	900	3.743	3.929	3.849	3.88	3.916	3.747
100	1000	3.636	3.915	3.847	3.878	3.893	3.743
100	1100	3.503	3.879	3.832	3.841	3.865	3.696
100	1200	3.536	3.871	3.823	3.784	3.839	3.69

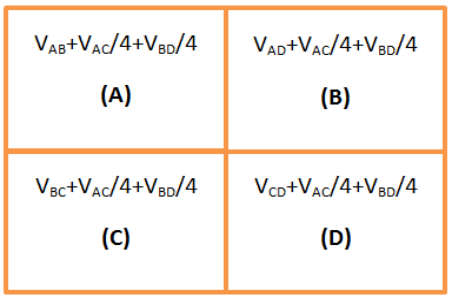

Figure 5.2 Assigned values of Array.

Based on the mathematical relationship portrays on Figure 5.2 each pixel values can be evaluated. Considering a scenario where DPF model is 25% fill means total fill is 300 gm. According to Figure 5.2 and voltage values from Table 5.1 pixel values of [A] pixel is calculated below

[A] Pixel value = VAB+VAC/4+VBD/4 = 3.9656 + (3.9549/4) + (3.87556/4) = 5.923215

Using this pixel values four detection images have been generated. Figure 5.3 and Figure 5.4 depicts some stages of soot deposition image.

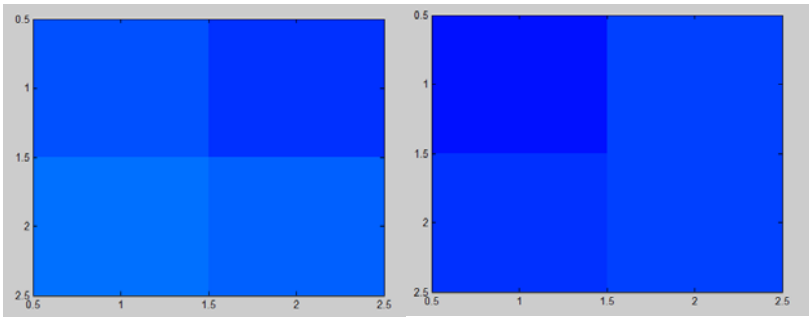

(a) DPF zero fill (b) DPF 25% fill

Figure 5.3 Rule based tomographic image of DPF with zero and 25% fill.

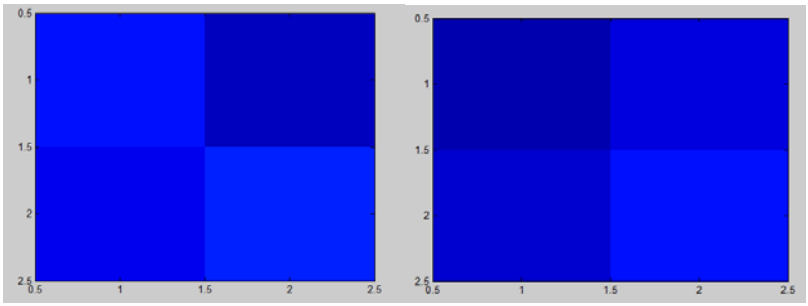

(a) DPF 50% fill (b) DPF 75% fill

Figure 5.4 Rule based tomographic image of DPF with 50% and 75% fill.

In both Figures 5.3 and 5.4 detection image showed significant changes with the material deposition.

5.2 Linear Back Projection Based Tomographic Image Generation

After generating primary deposition detection image the Linear back projection has been used to generate tomographic image which is quite a bit complex algorithm compare to our previous method. To create a tomographic image using linear back projection method sensitivity matrix has been created [29]. The complete set of a

measured inter-electrode capacitance values is required to reconstruct one permittivity distribution image. Figure 5.6 shows a 4*4 square pixel grid used to display the permittivity distribution image of a 4-electrode sensor, distributed as Figure 5.5, having circular intersection of Diesel particulate filter. From this (4*4) square pixel grid containing 16 pixels, all 16 are needed to construct the cross sectional image of the DPF.

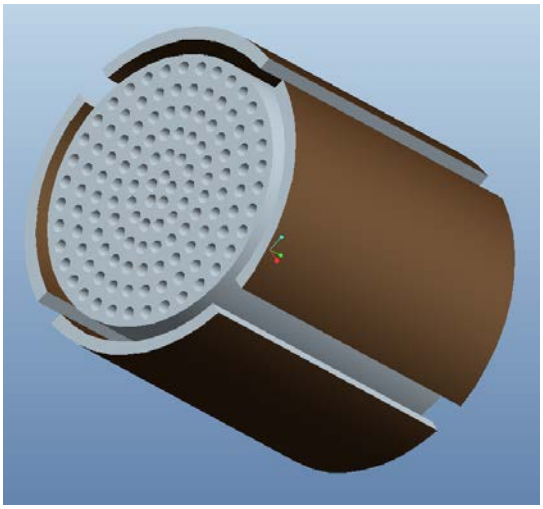

Figure 5.5 DPF with four capacitor plate.

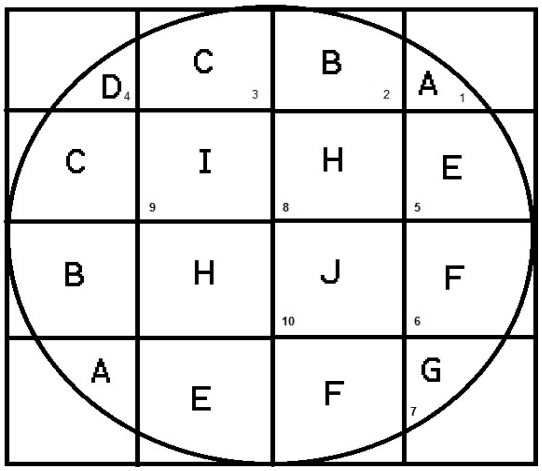

Figure 5.6 square pixel grid.

A proper sensitivity map, purpose of which is to aid in selecting the proper pixel that individually contributes to the capacitance changes, has been developed in Table 5.2 for visualizing the electric field established between two electrodes when one of them is excited.

Table 5.2 Sensitivity Map

PIXEL	A-B	A-C	A-D	B-C	B-D	C-D
A	3.692	3.638	3.550	3.670	3.641	3.944
B	3.685	3.635	3.556	3.662	3.680	3.830
C	3.554	3.657	3.600	3.644	3.649	3.868
D	3.537	3.578	3.669	3.637	3.671	3.487
E	3.540	3.644	3.593	3.582	3.657	3.884
F	3.555	3.678	3.641	3.664	3.717	3.934
G	3.597	3.599	3.539	3.562	3.615	3.893
H	3.528	3.645	3.642	3.643	3.687	3.971
I	3.659	3.623	3.577	3.651	3.678	3.976
J	3.509	3.638	3.636	3.671	3.710	3.975
A1	3.509	3.657	3.625	3.687	3.744	3.968
B1	3.702	3.666	3.618	3.646	3.719	3.591
C1	3.716	3.678	3.594	3.710	3.718	3.935
E1	3.535	3.646	3.564	3.688	3.698	3.993
F1	3.713	3.667	3.588	3.709	3.716	3.992
G1	3.626	3.657	3.569	3.658	3.661	3.970

Sensitivity map is one of the crucial parts of a tomographic image generation in LBP method. Sensitivity map needed to be created only for one calibration. For both end of the range of soot deposition to be measured the data in zero fill and then the data in complete fill has been obtained. These high and low data sets have been used to calibrate the sensor.

Once the sensor has been calibrated capacitance data during various loading cycle has been obtained and normalize. The method of normalization took place in single step. As for example one set data normalize has been shown below.

$$S_i(N) = \frac{C_i - C_i(emp)}{C_i(full) - C_i(emp)} \; fori = 1...M \; .$$

C_i (empty) = 3.82V and C_i (full) = 3.25V

From Table 5.2 a particular C_i = 3.55V

So S_i = (3.55 - 3.82) / (3.25 - 3.82)

S_i = 0.47 $(0 < S_i < 1)$

Based on this calculation Table 5.3 normalize sensitivity map has been generated using Table 5.2.

Table 5.3 Normalize Sensitivity Map

	A-B	**A-C**	**A-D**	**B-C**	**B-D**	**C-D**
A	0.928425	0.715134	0.186846	0.570407	0.348201	0.896534
B	0.912299	0.693707	0.217141	0.542215	0.557531	0.682336
C	0.615689	0.843042	0.445987	0.4767	0.393433	0.753609
D	0.577745	0.308856	0.804782	0.449124	0.51081	0.040341
E	0.584872	0.757605	0.408925	0.250021	0.435328	0.784783
G	0.619509	0.988106	0.657259	0.548826	0.760222	0.878138
H	0.033826	0.454527	0.131434	0.177413	0.209671	0.801636
I	0.556456	0.760303	0.664233	0.47097	0.598349	0.947324
J	0.37693	0.09076	0.063197	0.137947	0.101703	0.510613
A1	0.514518	0.71374	0.63178	0.572083	0.722203	0.954597
B1	0.514986	0.844774	0.577853	0.632677	0.90279	0.942237
C1	0.952372	0.90748	0.542103	0.48249	0.770144	0.234994
E1	0.983385	0.986083	0.416882	0.712909	0.764726	0.879863
F1	0.572664	0.769117	0.261937	0.635198	0.654436	0.989346
G1	0.975881	0.908155	0.385068	0.712414	0.753763	0.987084

After assembling the sensitivity map it was time to detect the change in material deposition inside DPF. How the soot has been distributed inside a DPF is still not been confirmed by any method. All diesel engine experts suggested that primarily soot deposited more densely near to the outer rim of the DPF because of the high speed entry into a DPF. Based on that approximation to measure soot deposition inside DPF two different approaches has been selected

a) 10% increment in soot load and

b) 20% increment in soot load.

Based on these approaches model DPF has been loaded with respect to time. After the completion of soot deposition inside the DPF one set of capacitance value has been measured. This set of experimental values after normalization multiplied with previously found normalized sensitivity map which brings us the pixel values according to linear back projection. The pixel values in the permittivity images are similarly normalized using the high and low pixel values so they have 0 for the lower value and 10 for the higher value. The permittivity distribution of the soot loading along circumference inside a DPF with 10% increment has been shown in Figure 5.7.

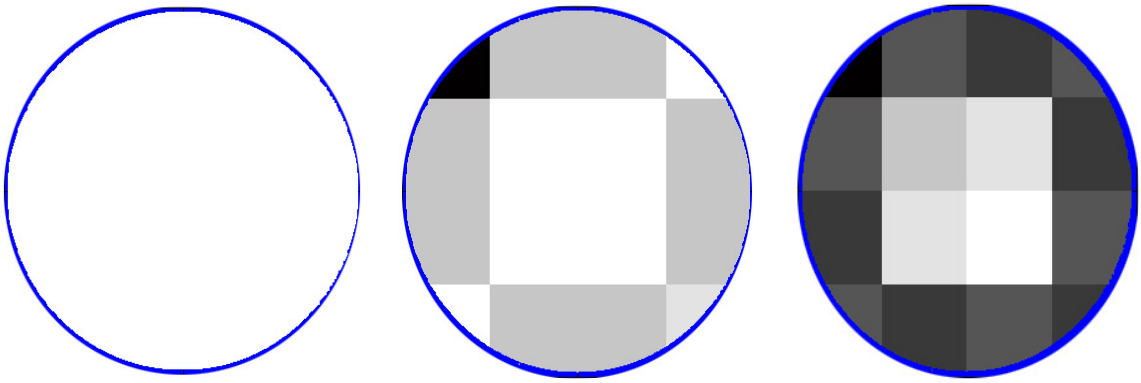

Figure 5.7 Tomographic images for 10% increment along circumference.

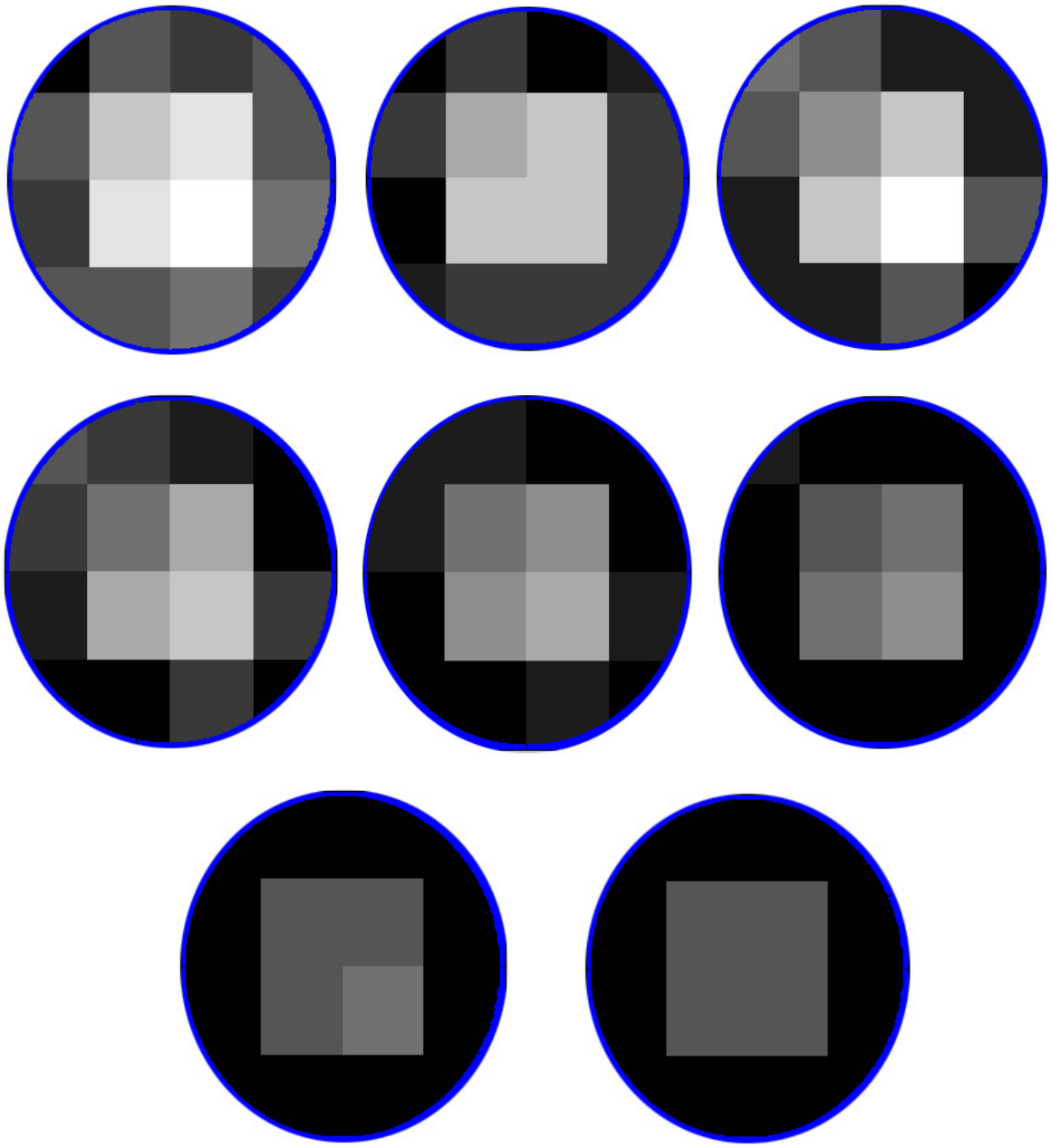

Figure 5.7 Continued.

The permittivity distribution of the Full soot loading inside a DPF with 10% increment has Shown different tomographic images than the soot loading along circumference. New Tomographic images been shown in Figure 5.8.

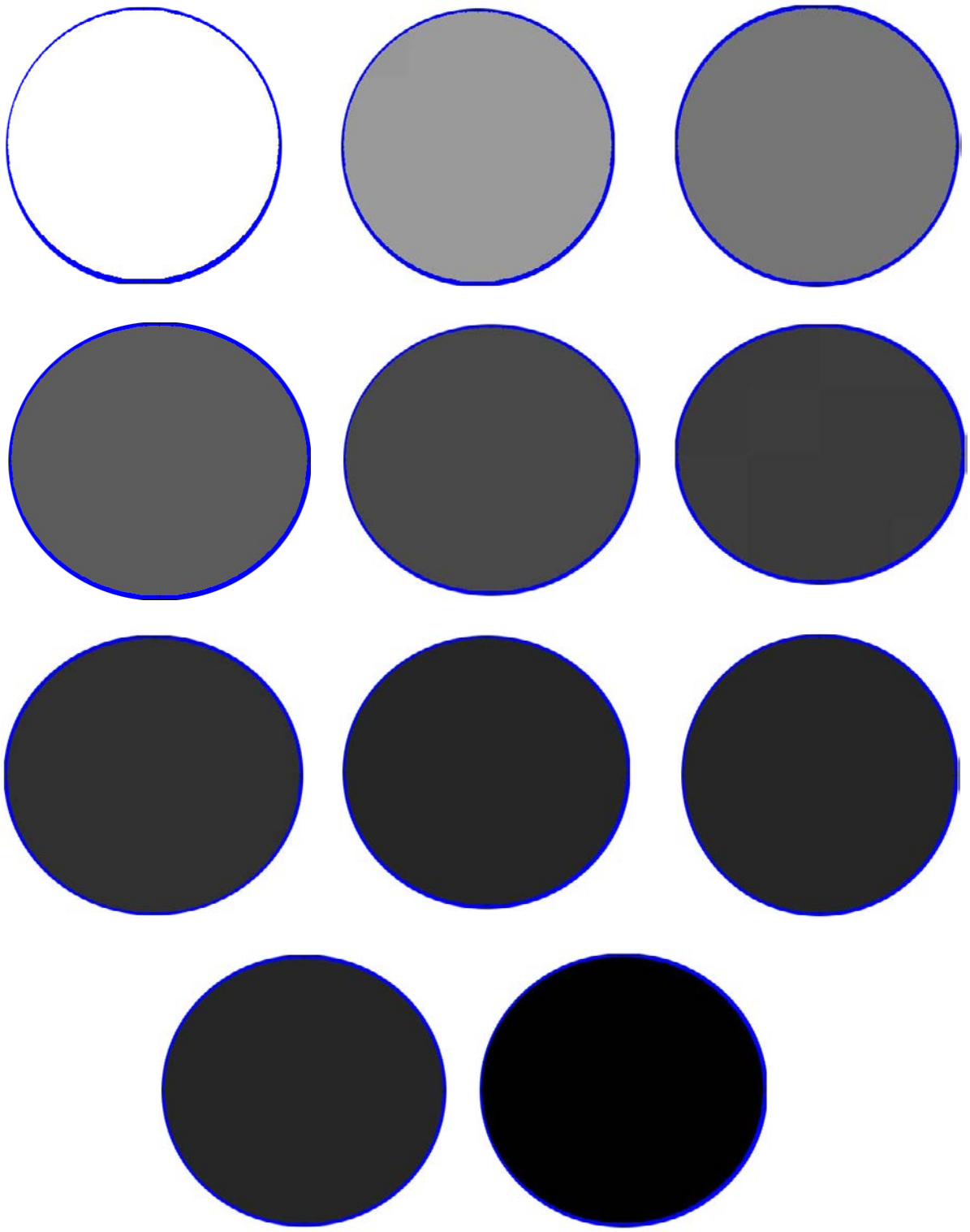

Figure 5.8 Tomographic images for 10% increment full.

The permittivity distribution of the soot loading along circumference inside a DPF with 20% increment has been shown in Figure 5.9.

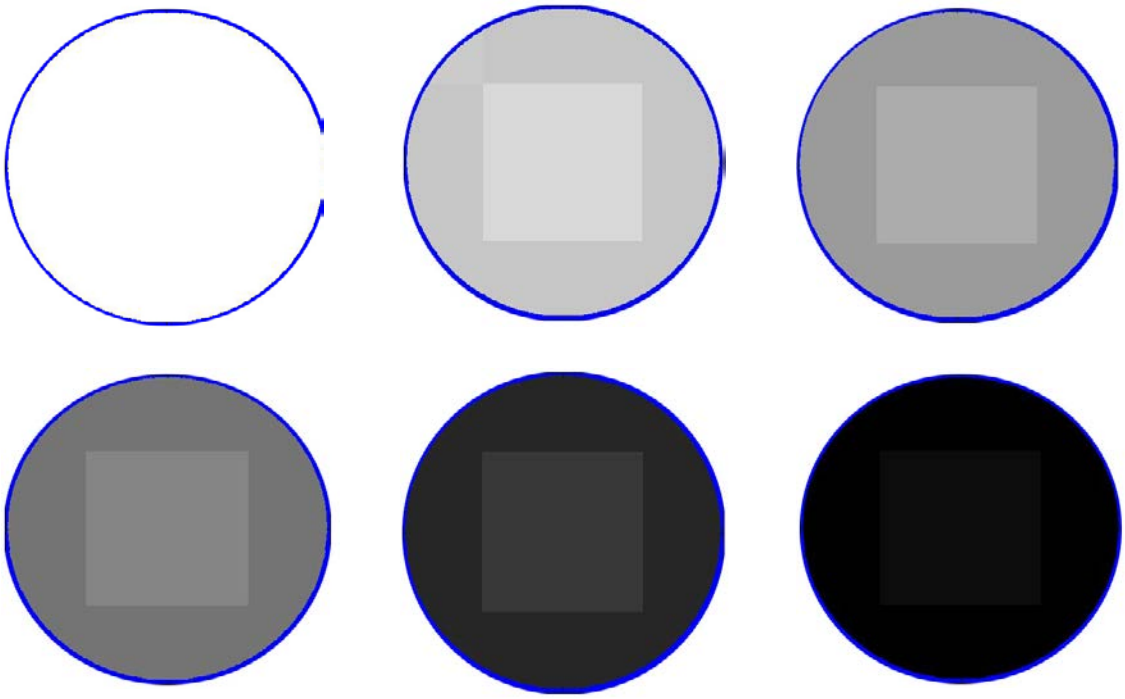

Figure 5.9 Tomographic images for 20% increment full along circumference loading.

The permittivity distribution of the Full soot loading inside a DPF with 20% increment has been shown in Figure 5.10.

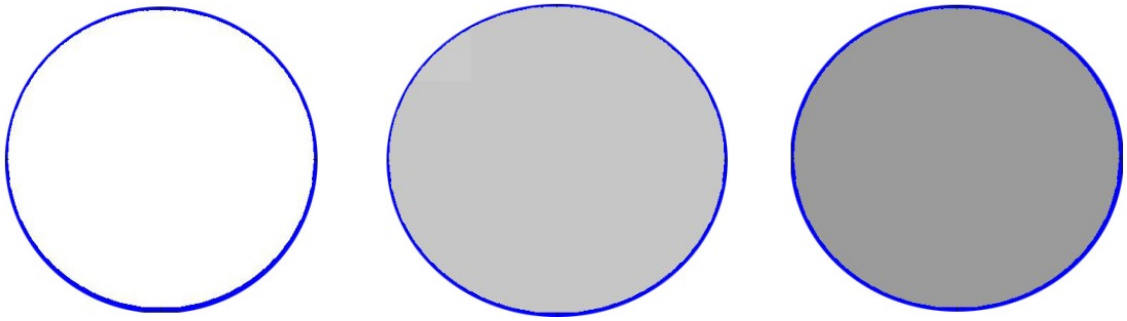

Figure 5.10 Tomographic images for 20% increment full loading.

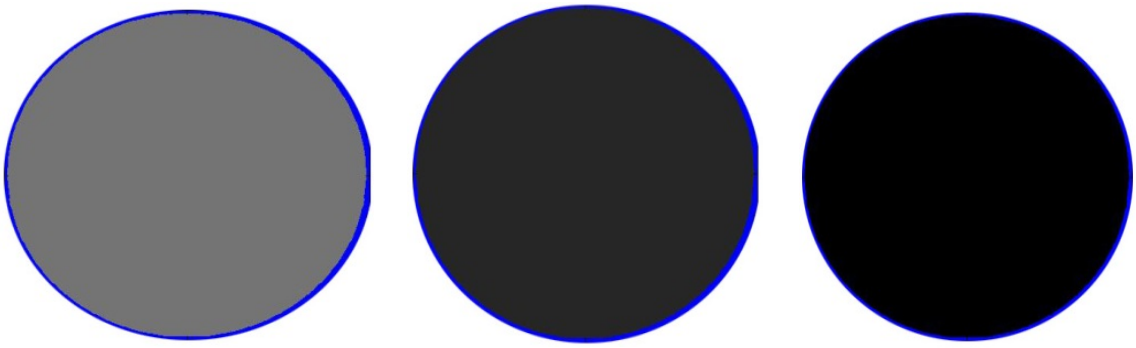

Figure 5.10 Continued.

From Figure 5.7 to 5.10 DPF tomographic images for different loading condition has been recorded. It's evident that tomographic images are capable of capture the soot deposition amount change. In Figure 5.7 and 5.8 tomographic images of last few stages shows similar color concentration, because at those stages the total mass of soot inside the DPF is so high that the detection voltage do not vary significantly, from Figures 4.2 and 4.3 plots these characteristics are evident. For more verification of the theory Printex U has been used for the experiment for soot replacement. Though dry sand does have similar dielectric properties of soot but pritex u material has more chemical similarities with soot.

5.3 Rule Based Tomographic Image Using Printex U Material

For experimentation of diesel emission Printex U always been used as a replacement of Diesel soot. After generating primary tomographic image using dry sand, Printex U has been used in the experimental setup to prove the theory in case of soot. For dry sand experiment results the changes in pixel density with the change is soot

deposition is quite high. In Table 5.4 the output voltages in ECT electrodes were shown using Printex U.

Table 5.4 Output voltage using Printex U

Weight gm	A-B	A-C	A-D	B-C	B-D	C-D
0	3.6294	3.7088	3.6825	3.7547	3.7865	3.6789
18.7	3.5779	3.6219	3.5363	3.6439	3.6878	3.5933
18.7	3.3428	3.4265	3.3828	3.5889	3.6612	3.5668
18.9	3.2675	3.3525	3.3658	3.4256	3.5254	3.4864
19	3.2675	3.3665	3.1920	3.3738	3.3451	3.2780
18.8	3.1747	3.3279	3.1137	3.1090	2.9336	3.1940
19.4	2.7117	3.2547	3.0503	2.8826	2.8642	3.1044
19.9	2.2951	3.0660	2.9979	2.8242	2.8516	3.0916
20.3	2.2853	3.0369	2.9934	2.8196	2.8501	3.0782
19.4	2.2708	3.0202	2.9763	2.7988	2.8430	3.0775
18.9	2.2238	2.8842	2.8527	2.6458	2.7083	2.9343
20	2.2192	2.5984	2.4190	2.5135	2.5438	2.6997

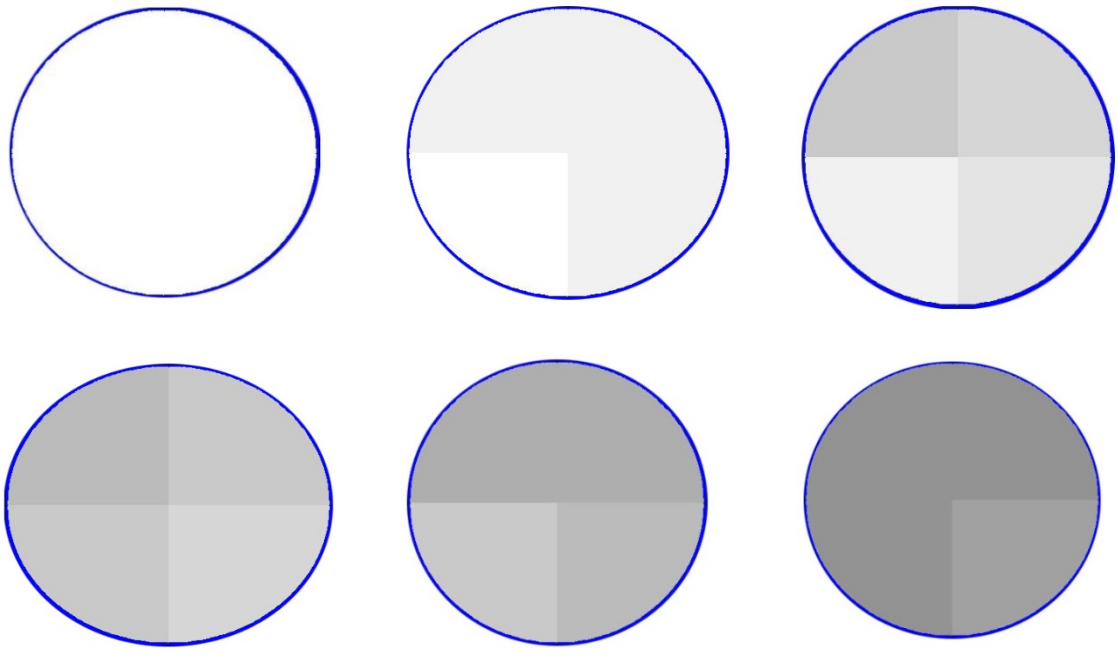

Figure 5.11 Rule based tomographic image using Printex U.

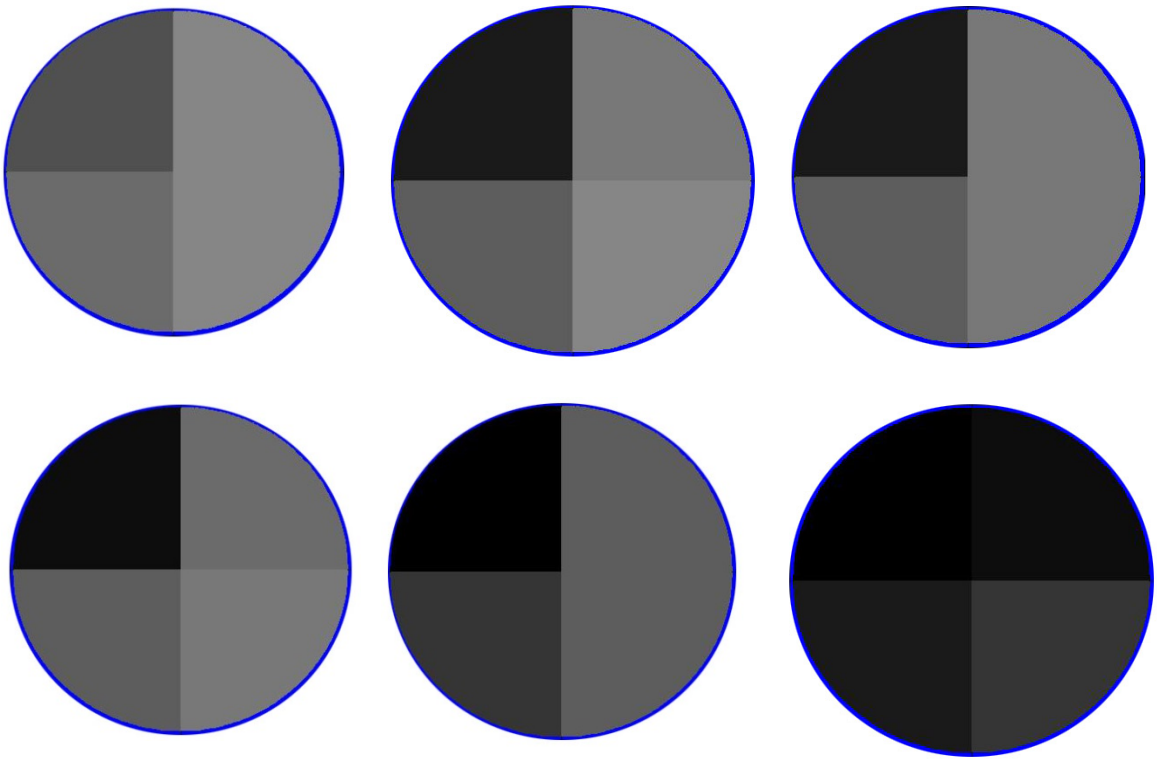

Figure 5.11 Continued.

From Figure 5.11 tomographic images its evident that presence of soot inside a DPF can be detected using rule based method but location of soot deposition are not conclusive, because instead of uniform soot deposition tomographic image shows high concentration of soot deposition in one particular quadrant which is quite unlikely. So it's evident that to detect soot location with soot detection a more robust method has to be implemented, at that point again LBP method comes in. LBP helps to create tomographic images of DPF with the help of sensitivity pixels so location of soot deposition is also possible. Though previously in this work LBP method has been used to prepare tomographic image for dry sand, it will be visible that for Printex U material the tomographic image will be more vivid.

5.4 Linear Back Projection Based Tomographic Image Using Printex U

Though dry sand is not very close of original soot but for experimentation use of dry sand increase the flexibility. Eventually when Printex U has been used as a soot replacement then more vivid voltage difference is visible compare to dry sand. Following Figure 5.12 all electrode voltage differences between soot and dry sand has been displayed.

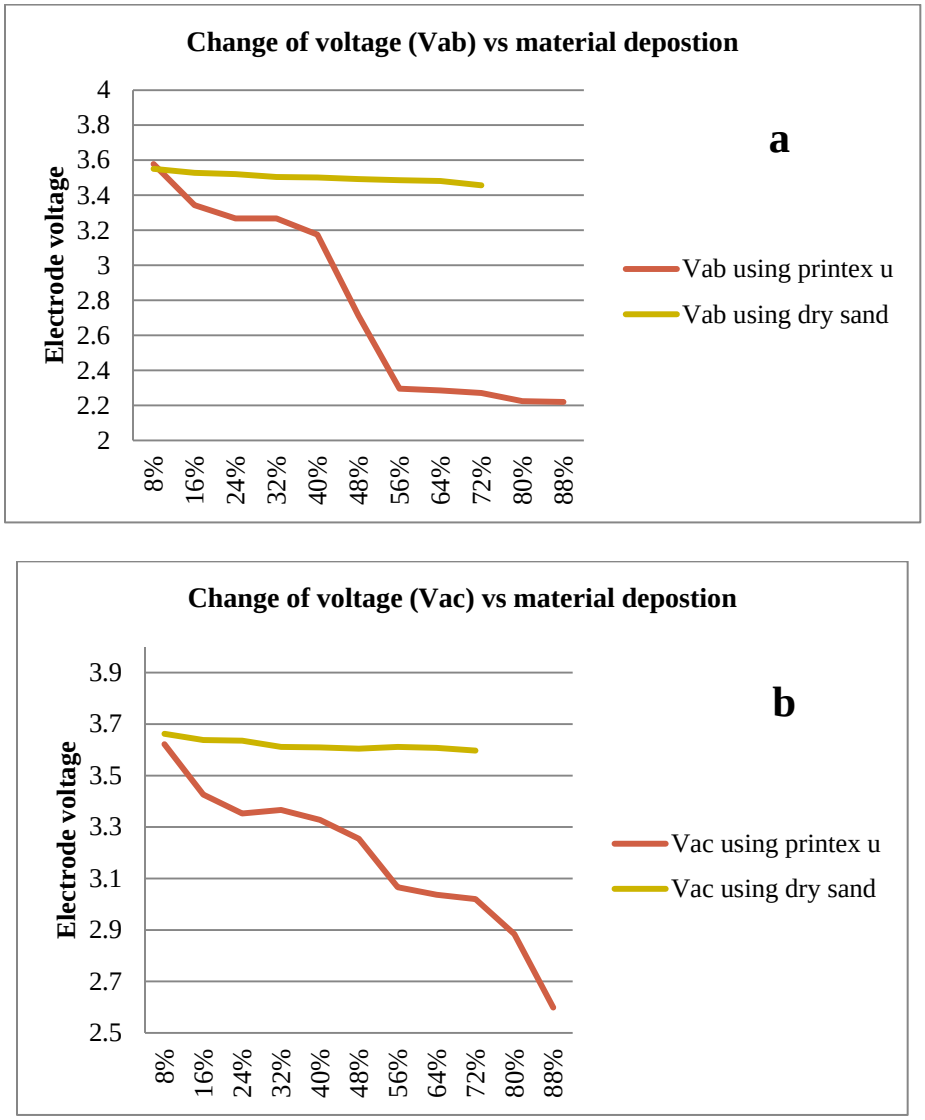

Figure 5.12 All set of n of Electrode Voltage differences between Printex U and dry sand (represents by a to f).

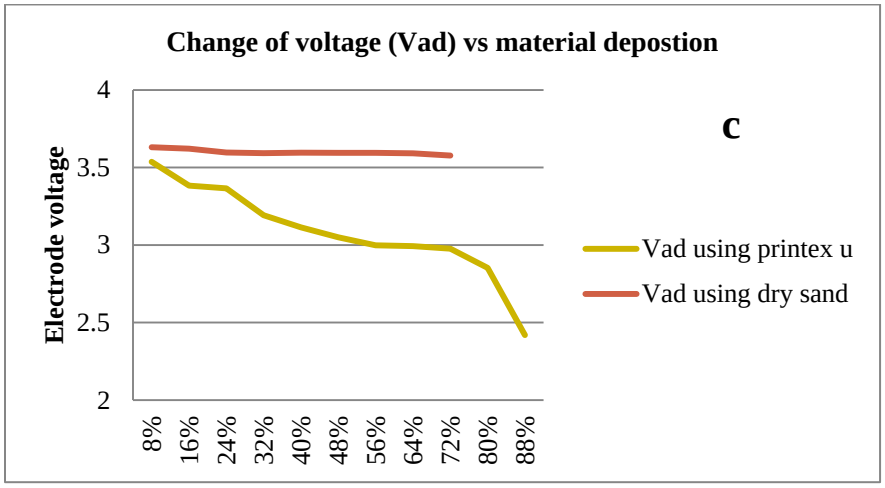

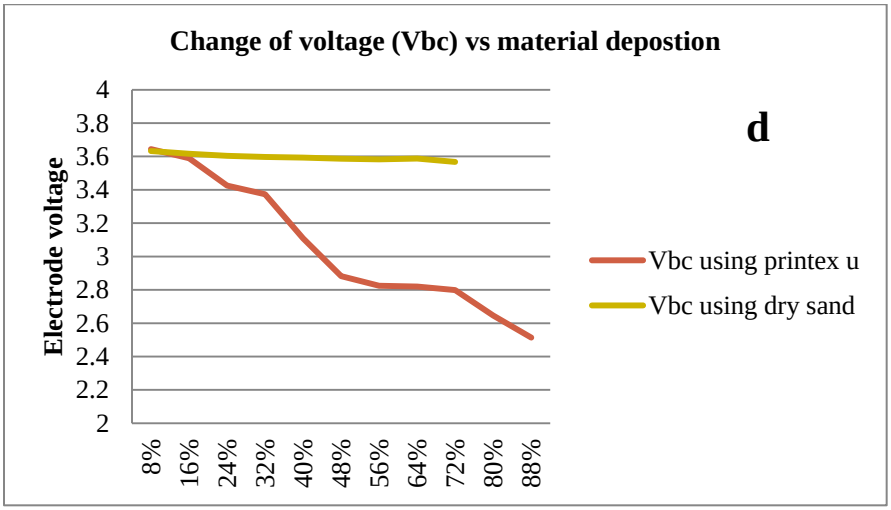

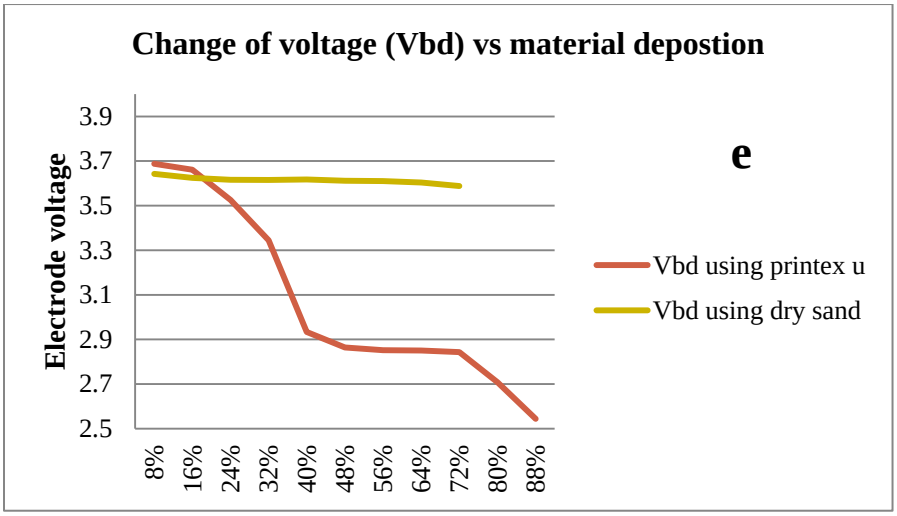

Figure 5.12 Continued.

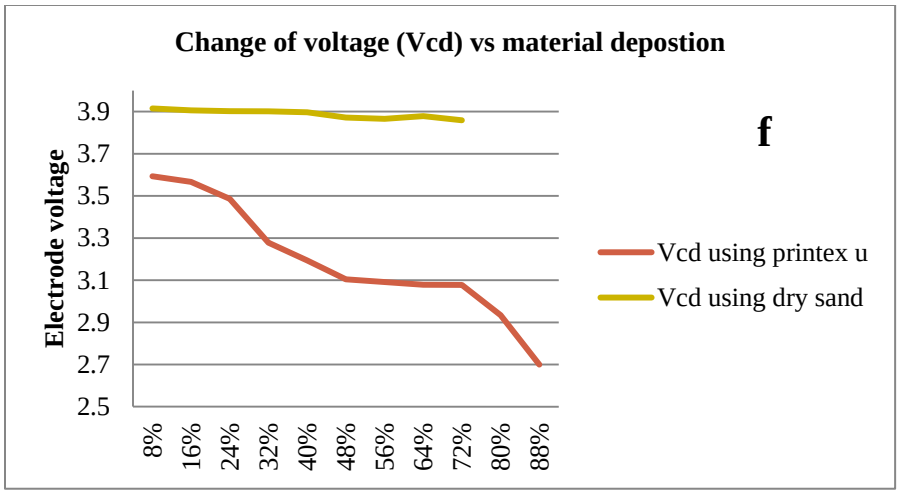

Figure 5.12 Continued.

From Figure 5.12 all voltage output comparison it is visible that voltage changes due to Printex U deposition inside the DPF is more vivid than dry sand deposition. Usually dry sand addition causes voltage change range from 3.95V to 3.75 V. On the other hand Printex U deposition causes voltage change range to shift to 3.7V to 2.2V, though with the increase of the range linearity of the output voltage diminishes. This Increase of voltage range cause better data acquisition and more versatile range of soot deposition can be recorded.

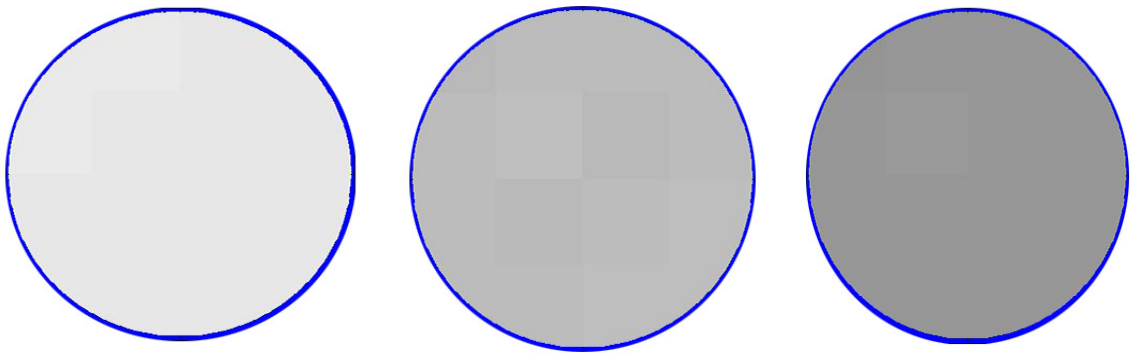

Figure 5.13 Tomographic image using Printex U full loading.

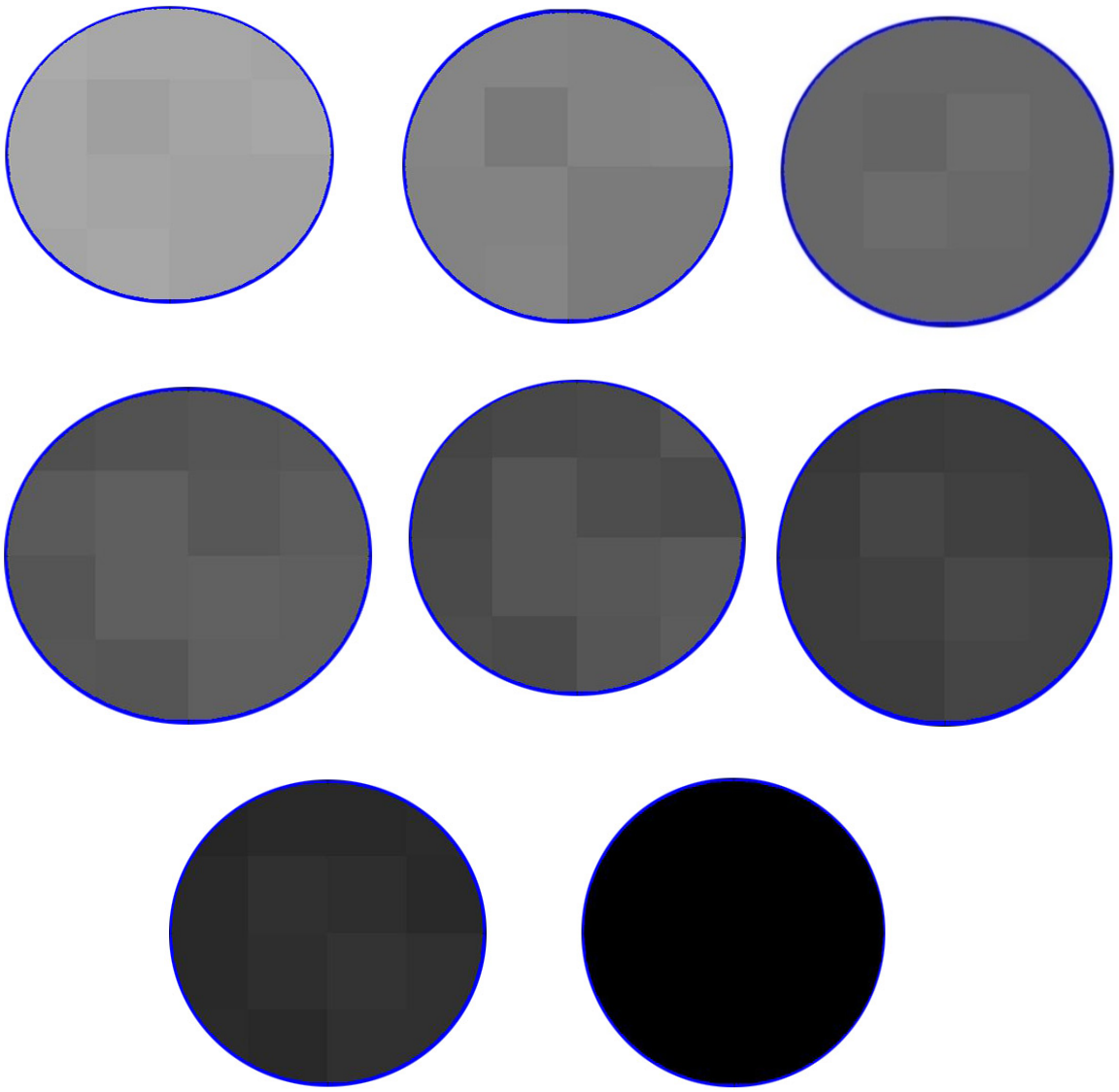

Figure 5.13 Continued.

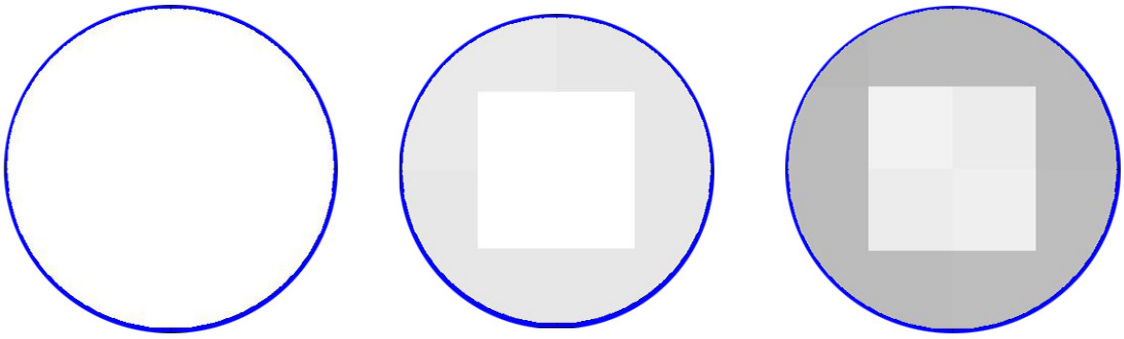

Figure 5.14 Tomographic image using Printex U circumferential loading.

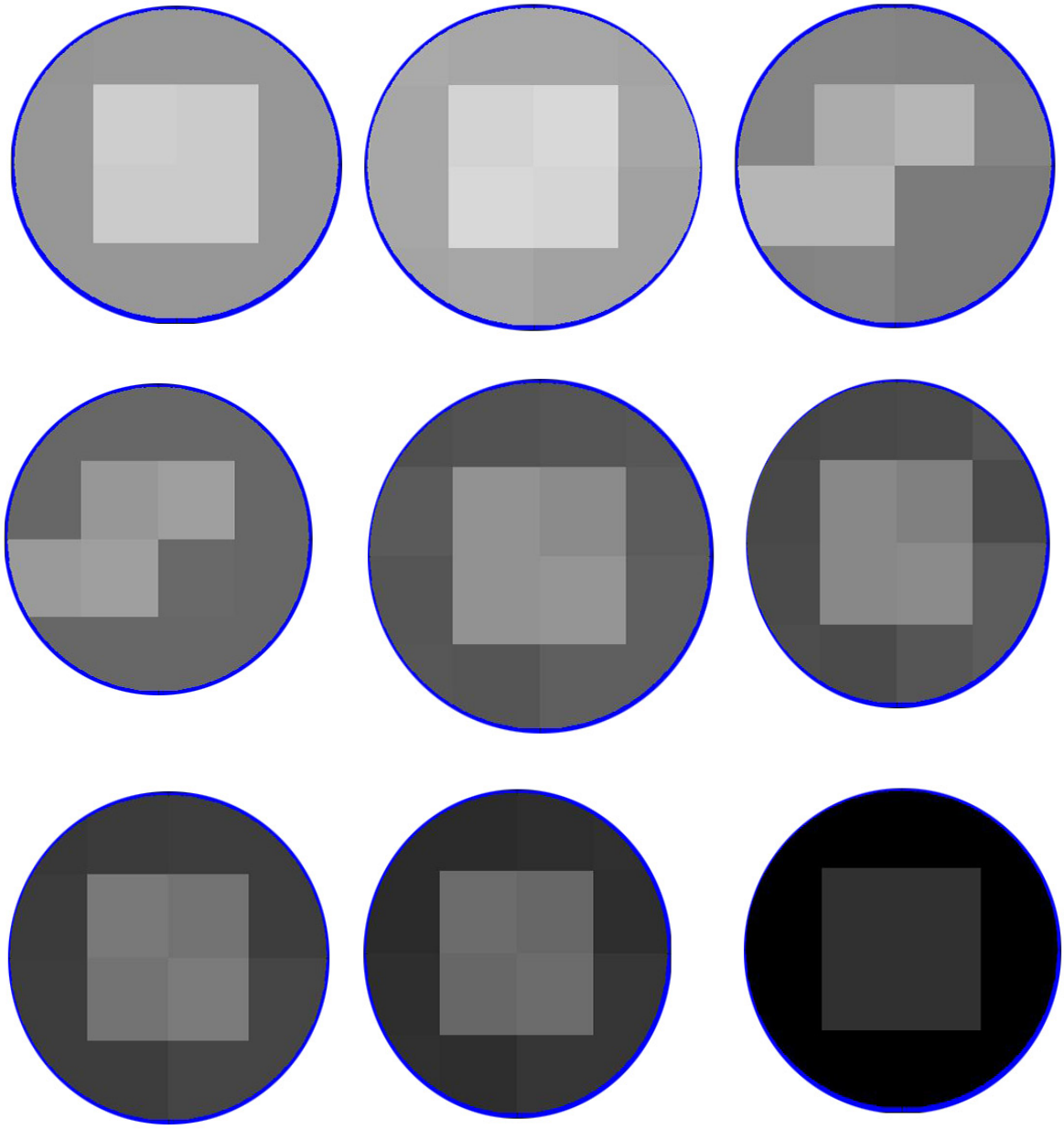

Figure 5.14 Continued.

Comparing between Figure 5.7-5.10 (dry sand tomographic image) and Figure 5.13-5.14 (Printex U tomographic image) shows that due to bigger voltage output range Printex U deposition can give much better image contrast during tomographic image

generation. Again comparing Figure 5.13 and 5.14 with Figure 5.11 (rule based image formation), contrast between pixels shows that LBP method is more accurate method.

5.5 Statistical Error Calculation in Output Voltage

In order to verify the accuracy in the result or to check the repeatability, statistical analysis has been conducted on the experimental results. Primarily for dry sand and 10-90% soot loading condition, all the experimental voltage results of capacitance V_{AB} has given at Table 5.5 and Table 5.6 has presented the mean, standard deviation and standard error for same voltage results.

Table 5.5 Output voltage V_{ab} using dry sand

Material Deposition %	**DATA (a)**	**DATA (b)**	**DATA (c)**	**DATA (d)**	**DATA (e)**	**DATA (f)**	**DATA (g)**	**DATA (h)**	**DATA (i)**
10	3.599	3.601	3.578	3.543	3.588	3.529	3.590	3.530	3.591
20	3.599	3.572	3.568	3.512	3.588	3.525	3.568	3.514	3.500
30	3.593	3.558	3.545	3.508	3.564	3.510	3.558	3.490	3.483
40	3.502	3.526	3.501	3.478	3.533	3.506	3.465	3.484	3.476
50	3.491	3.501	3.496	3.453	3.525	3.486	3.458	3.480	3.463
60	3.482	3.495	3.475	3.390	3.484	3.471	3.446	3.472	3.452
70	3.465	3.466	3.471	3.387	3.469	3.436	3.413	3.381	3.401
80	3.452	3.422	3.459	3.384	3.465	3.409	3.409	3.374	3.393
90	3.430	3.415	3.386	3.384	3.419	3.388	3.391	3.366	3.385

Table 5.6 Standard deviation and error

Material Deposition %	Mean	SD	Standard error
10	3.572	0.028	0.009
20	3.550	0.035	0.012
30	3.535	0.036	0.012
40	3.499	0.023	0.008
50	3.485	0.022	0.007
60	3.465	0.030	0.010
70	3.434	0.036	0.012
80	3.417	0.032	0.011
90	3.393	0.021	0.007

Table 5.5 has represented the fact that experimental shows pretty high repeatability with a very low standard error. Following same steps Output voltage V_{ab} using Printex u, standard deviation and error has been recorded in Table 5.7 and Table 5.8.

Table 5.7 Output voltage V_{AB} using Printex U

Material Deposition %	DATA 1	DATA 2	DATA 3	DATA 4	DATA 5	DATA 6	DATA 7	DATA 8	DATA 9
9	3.628	3.454	3.549	3.542	3.471	3.525	3.460	3.565	3.513
18	2.839	3.339	3.381	3.481	3.218	3.389	3.374	3.506	3.049
27	2.807	3.335	3.378	3.449	3.019	3.266	3.269	3.374	2.907
36	2.647	3.248	3.334	3.153	3.019	3.070	3.170	3.313	2.851
45	2.479	3.041	3.155	3.070	2.778	3.062	3.067	3.139	2.806
54	2.429	2.938	3.122	2.844	2.705	3.062	3.044	3.102	2.806
63	2.409	2.832	2.968	2.772	2.649	2.754	2.889	3.088	2.779
72	2.390	2.726	2.893	2.653	2.560	2.664	2.859	2.726	2.614
81	2.318	2.426	2.677	2.584	2.523	2.243	2.573	2.698	2.571

Table 5.8 Standard deviation and error

Material Deposition %	Mean	SD	Standard Error
9	3.514	0.057	0.018
18	3.265	0.204	0.065
27	3.182	0.213	0.067
36	3.075	0.206	0.065
45	2.952	0.200	0.063
54	2.854	0.237	0.075
63	2.751	0.215	0.068
72	2.642	0.170	0.054
81	2.493	0.150	0.047
90	2.356	0.136	0.043

Table 5.8 represents the facts that during the experiments the standard errors are pretty less, and the errors ranges from 0.018 to 0.067. Another method to check the repeatability is to check the frequency of a certain result range. Again for dry sand voltage output result frequency has been plotted in Figure 5.15.

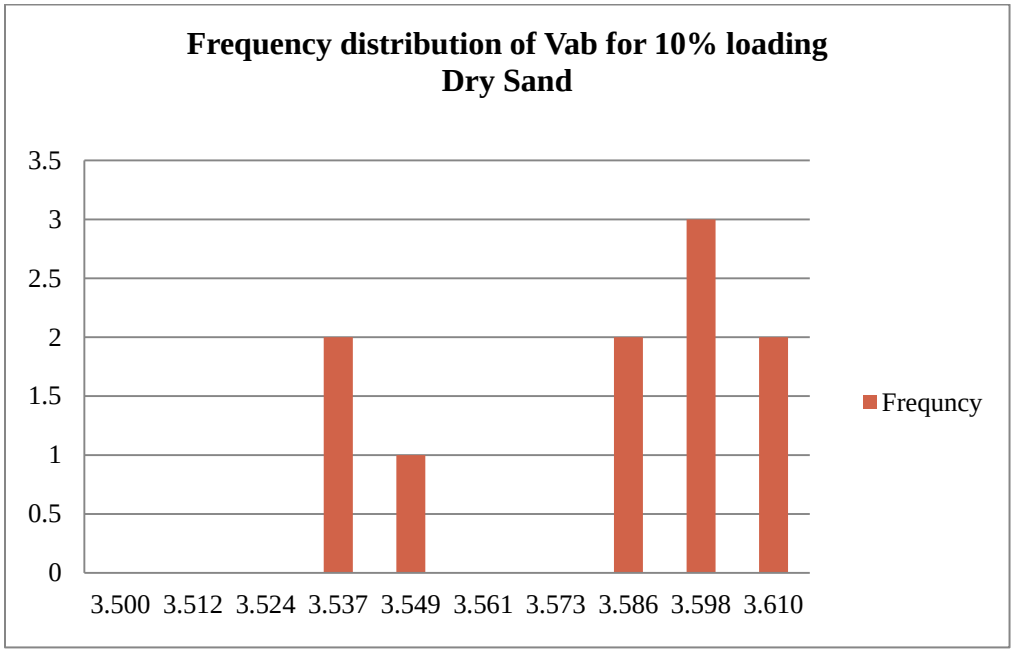

5.15 Frequency distribution for dry sand.

And for Printex U voltage output result frequency has been plotted in Figure 5.16.

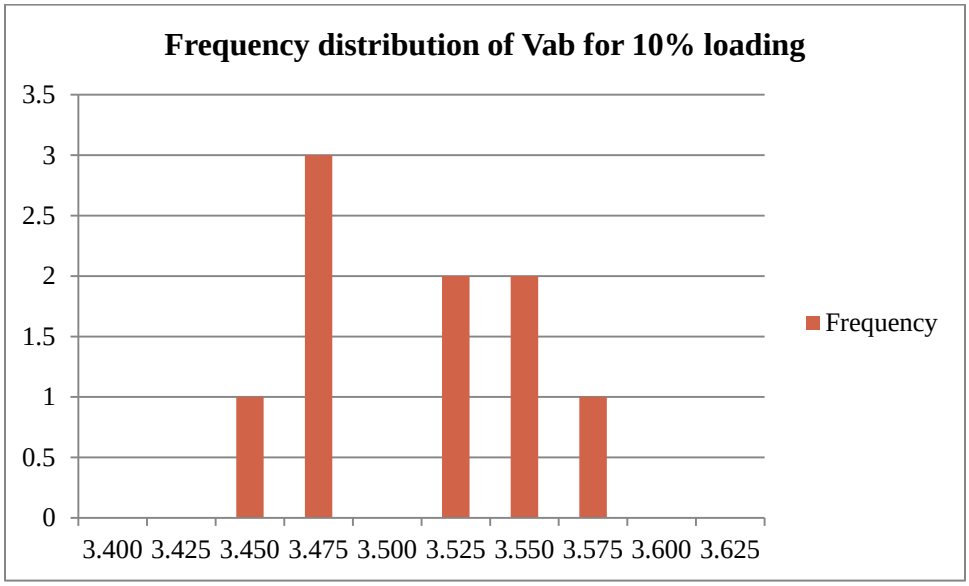

5.16 Frequency distribution for Printex U.

Figure 5.15 and Figure 5.16 shows very small irregularities in the result of $V_{ab.}$ Frequency of the voltage values varies, and that variation causes the irregularities in voltage vs deposition curve like Figure 4.2 and 4.3 or in the tomographic images.

6. CONCLUSION AND FUTURE WORK

6.1 Conclusion

Diesel particulate filter is a very important inclusion in a diesel engine to maintain the emission level per standard. Though there are several types of DPF technologies are available in the market this paper focuses on the model closest to cordierite diesel filter. Most of the DPF currently available in the market can reduce PM emission almost 99%. But only soot deposition is not the only purpose of DPF, after few cycles the soot has to burn down completely to eliminate the Pm from DPF. That require very high temperature which can cause cracks inside the DPF surfaces and excessive fuel use can cause fuel penalty. To maintain an optimized amount of fuel for PM burning accurate knowledge of deposited soot in necessary. For both maintain DPF structural integrity and maintain emission regulation it is very important to know the exact amount soot deposited inside a DPF. There are several technologies available to detect and measure the soot status inside a DPF like pressure drop sensor, particulate emission sensor, microwave sensor, radio frequency sensor etc. In this paper we discussed about a novel soot sensing sensor based on electrical capacitance tomography. Previously ECT system has been used in various purposes like two flow concentration measurements in oil industries but in this paper ECT has been implemented on DPF soot measurement system where any soot or Particulate Matter deposition inside DPF will cause a change in total dielectric properties

inside the DPF. This of dielectric property will cause a change in the capacitance. Electrodes of ECT system are going to act a set of capacitor surrounded the DPF. Whenever there is a change of dielectric property inside a DPF the changes will be captured via capacitors surrounded it. A set of capacitor will capture a combination of capacitance data and voltage data. After applying either rule based method or linear back projection method a tomographic image of a particular state can be captured.

For this paper primarily, as soot replacement Printex U has been used because it has the closest dielectric property of original soot, and this material is available in market. After running the simulation and primary capacitance experiment it is evident that change in the deposition material can change the capacitance. After getting the proof of this theory ECT system in a model DPF, made of Nylon 66), has been implement with a dry sand distribution and captured results. After finishing the experiment using dry sand a different type of material has been used for experimentation. Printex U has closest chemical properties of soot originally generated from an engine. After using Printex U primary data showed more dynamic result compare to dry sand results. Whole experiment has been repeated using Printex U and this time we have received more vibrant tomographic images with more contrast.

The simulation results demonstrated the general relationship between the amount of soot deposited and the output voltage of ECT system and experimental results shows that ECT systems are responsive with the change of material accumulation thickness. To be more specific, from previous papers and experimental results its evident that deposited soot thickness inside DPF will cause varying dielectric constant which will impact the capacitance of ECT system and output voltage. And the final tomographic images of both

from dry sand and Printex U material showed that detection of soot deposition inside a DPF is possible using this ECT technology.

6.2 Future Work

The experimental works related with this paper solely has the proof of the theory. Electrical Capacitance tomography is a very comprehensive method which can be implemented in any multiphase flow concentration measurement. Some future works has been mentioned below

1. Transient analysis

All the experiments involved in this paper are conducted in a steady state mode. To take this study further a transient analysis of soot deposition measurement using ECT system has to be conducted. Transient analysis should be involved with various types of driving cycles. For conducting the experiments in a transient form a complete setup of engine and engine after treatment system will be prepared.

2. Finite Element Analysis (FEA) Analysis

A numerical technique like Finite Element Analysis can be implemented to measure the soot deposition amount changes inside a diesel particulate filter. Using FEA a bigger sensitivity matrix can be generated which will generate tomographic images with higher contrast.

3. Hardware In loop (HIL) Simulation

Using HIL simulation an interface between the plant simulation and embedded system can be created. This embedded system can be used to test the real complex systems.

4. Analyze external impact

Outside temperature pressure and humidity does have some impact on the overall engine performance and including engine emission, so external factors have some impacts on the ECT system output results. Environmental impact has to be tested on DPF soot measurement system

5. Error calculation

After developing an original engine setup and original DPF in a test bed a neutron based or TEOM based nondestructive tests can be implemented to measure the exact error percentage of soot deposition result inside a DPF.

6. Model based fault detection

A model based fault detection method can be implemented to detect any crack and internal flaws of a DPF. A simplified model development will be the work for next stage then comparing results from model with experimental data can lead to a very robust DPF fault diagnosis method.

LIST OF REFERENCES

LIST OF REFERENCES

[1] M. Twigg and P. R. Phillips, “Cleaning the air we breathe—controlling diesel particulate emissions from passenger cars,” in Platinum Metals review, Volume 53, Issue 1, Jan 2009, Pages 27-34.

[2] J. Adler, “Ceramic diesel particulate filters,” in International of Journal Applied Ceramic Technology, Volume 2, issue 6, 2005, Pages 429–439.

[3] G. Fischerauer, M. Forste and R. Moos, “Sensing the soot load in automotive diesel particulate filters by microwave methods,” in Measurement Science and Technology, volume 21, 2009, Pages 235-247, number 3.

[4] A. Sappok, L. Bromberg, J. Parks and V. Prikhodko, “Loading and Regeneration Analysis of a Diesel Particulate Filter with a Radio Frequency-Based Sensor,” in SAE Technical Paper, San Diego, California, 2010, Pages 27-34.

[5] H. Husted, G. Roth, S. Nelson, L. Hocken and G. Fulks, “Sensing of Particulate Matter for On-Board Diagnosis of Particulate Filters,” in SAE International Journal of Engines, Volume 5, issue 2, 2012, Pages 235-247.

[6] N. Ohyama, T. Nakanishi and S.Daido, “New Concept Catalyzed DPF for Estimating Soot Loadings from Pressure Drop,” SAE Technical Paper 2008-0620.

[7] N. Singh, C. Rutland, D. Foster and K. Narayanaswamy, “Investigation into Different DPF Regeneration Strategies Based on Fuel Economy Using Integrated System Simulation,” SAE Technical Paper 2009-01-1275, 2009.

[8] D. Rose and T. Boger, “Different Approaches to Soot Estimation as Key Requirement for DPF Applications,” in SAE Technical Paper, Detroit, Michigan, 2009, DOI: 10.4271/ 2009-01-1262.

[9] A. Strzelec, H. Bilheux, C. Finney and C. Daw, “Neutron Imaging of Diesel Particulate Filters,” in SAE Technical Paper, San Antonio, Texas, 2009.

[10] R. L. Boylestad, “Capacitor,” in Introductory Circuit Analysis, 11th ed. New Jersey, USA: Pearson Prentice Hall, 2007, ch. 10, sec. 10.3, pp. 398–410.

[11] S. Donthi, “Capacitance based Tomography for industrial Applications,” M.Tech. Thesis, Electrical Engineering Dept., IIT, Bombay, 2004.

[12] M. Koledintseva, R. DuBroff and R. Schwartz, “A Maxwell Garnett model for dielectric mixtures containing conducting particles at optical frequencies,” in Progress in Electromagnetics Research, Vol. 63, 2006, pages 223-242.

[13] Z. Cao, L. Xu, W. Fan and H. Wang, “Electrical capacitance tomography for sensors of square cross sections using Calderon’s method,” IEEE Trans. Instrum. Meas., vol. 60, no. 3, pp. 900–907, Mar. 2011.

[14] Y. Wuqiang, “Design of electrical capacitance tomography sensors,” in Measurement Science and Technology, Volume 21, Number 4, 2010.

[15] J. C. Gamio, c. Ortiz-Alemán and R. Martin, “Electrical capacitance tomography two-phase oil-gas pipe flow imaging by the linear back-projection algorithm,” in Geophysical International, Volume 44, issue 3, 2005, Page number 265-273.

[16] Electrical Capacitance Tomography System Type Tflr5000 Operating Manual, Volume 1. Fundamentals of ECT, Process tomography ltd., England. 2009.

[17] R. Michel, R. Baican and E. Schubert, “Soot particle properties in the microwave range,” Retrieved from Microwave Conference, 1993. 23rd European, pages 959 – 960, Madrid, Spain.

[18] Matweb, Material Property data. Available: http://www.matweb.com/.

[19] Ferro Ceramic Grinding, Inc. Available http://www.ferroceramic.com/.

[20] L. Pryuor, R. Sclobohm and B. Brownell, “A comparison of aluminum vs. copper as used in electrical equipment,” Available FTP: https://www.geindustrial.com /sites/geis/files/gallery/, GE Consumer & Industrial website.

[21] A. Pyzik and C. Li, “New design of a ceramic filter for diesel Emission Control Application,” in International Journal of Applied Ceramic Technology, Volume 2, Issue 6, 2005, Pages 440-451.

[22] R. Waterfall, R. He, N. White and C. Beck, “Combustion imaging from electrical impedance measurements,” Meas. Sci. Technol. 7 369-74, 1996.

[23] W. Yang, A. Chondronasios, V. Nguyen, S. Nattras, M. Betting and I. Ismail, “Adaptive calibration of a capacitance tomography system for imaging water droplet distribution,” Flow Meas. Instrum. 15 249-58, 2004.

[24] W. Yang, A. Stott, M. Beck and G. Xie, “Development of capacitance tomographic imaging systems for oil pipeline measurements,” Rev. Sci. Instrum. 66 4326-32, 1995.

[25] T. Yakowski, M. Miko, D. Vlaev, R. Mann, G. Follows, A. Boxman and M. Wilson, “Imaging nylon polymerisation processes by applying electrical tomography,” Proc. 1st World Congress on Industrial Process Tomography (Buxton, UK, 14-17 April) pp 383-7 1999.

[26] E. S. Berney and D.M. Smith. (2008, February), “Mechanical and Physical Properties of ASTM C33 Sand [Type of medium],” Available: http:// www.dtic. mil/.

[27] B. Domenick, “A Graphical Sinusoidal Analysis of a Nonlinear RC Phase-Shift Feedback Circuit,” in Proceedings of the IRE, Volume 43, issue 6, June, 1955, page: 679-684.

[28] T. Fountain, “Software advances in measurement and instrumentation,” in IEE Colloquium on Software Instrumentation – Software Components, Feb, 1993, pp. 1-45.

[29] A. Rerkratn, K. Chitsakul, A. Soisup and V. Wuti, “Electrical capacitance tomography system for monitoring process flow in pipe,” in SICE Annual Conference 2010, Proceedings of, Taipei, China, 2010, page: 3229-3232.